SLAC-152
UC-34
(EXP) (EXPI)

THE SOLENOID VERTEX SPECTROMETER – A SIMULATION STUDY

GEORGE JURIS LUSTE*
STANFORD LINEAR ACCELERATOR CENTER
STANFORD UNIVERSITY
Stanford, California 94305

PREPARED FOR THE U.S. ATOMIC ENERGY
COMMISSION UNDER CONTRACT NO. AT(04-3)-515

June 1972

Printed in the United States of America. Available from National Technical Information Service, U. S. Department of Commerce, 5285 Port Royal Road, Springfield, Virginia 22151. Price: Printed Copy $3.00; Microfiche $0.95.

* Presently at the University of Toronto, Toronto 5, Ontario, Canada.

ABSTRACT

This study examines the particle detection characteristics of a large solenoid magnet and spark chamber system by means of Monte Carlo simulation. Such a device would serve as a vertex spectrometer in a two magnet system.

The nominal parameters are: a 25 kG axial field, a 2 meter diameter and a 3 meter length. The solenoid magnet can surround the target and measure the low momentum, large angle particles and a second magnet downstream, with a conventional gap and field would measure the fast secondaries. The axial field solenoid has ideal azimuthal symmetry and is well suited for rotating the transverse momentum vector of slow particles in hadron interactions.

A detailed study of the acceptance, momentum resolution and pattern recognition properties of the solenoid system are presented. The overall conclusions are that it can measure most particles of 2 GeV/c or less very well, improve overall acceptances dramatically, fill in dead regions of decay distributions, make high invariant mass studies feasible (8 to 16 GeV/c beams) and present no obvious difficulty for the pattern recognition of tracks. A fast track recognition algorithm is presented and no major computing needs are anticipated for the magnetic field inside the solenoid.

ACKNOWLEDGEMENTS

This publication would not have been possible without the encouragement and direct aid of a number of people.

Leon Madansky first introduced me to the spectrometer ideas and problems while on a sabbatical at SLAC. Together we explored some of the acceptance kinematics of a dipole magnet and a solenoid magnet system. This early collaboration was an invaluable learning experience for the author and it was at this suggestion that we first considered some simple solenoid kinematics in December of 1968.

David Leith has provided the support and encouragement to make the study comprehensive enough for a real spectrometer proposal. Without him, and his desire to build a good spectrometer facility this study could not have taken root. His enthusiasm and advice along the way did much to sustain it.

A number of my fellow colleagues at SLAC have also provided useful comments and advice during the course of this work. They are Jim Loos, Bob Carnegie, Kei Moriyasu, and Bill Johnson. John Matthews was kind enough to read the original draft of this report.

Chuck Stoner and Dave Budenaers helped with some of the calculations and computer programming.

TABLE OF CONTENTS

LIST OF TABLES

LIST OF FIGURES

I. INTRODUCTION

This report examines the feasibility of using a larger aperture high field solenoid magnet as a vertex spectrometer.

The study is essentially a software simulation of the possibilities of such a device. The limitations imposed by this objective should be kept in mind. At no point is there any discussion of the mechanical, cryogenic, electronic or cost estimate difficulties of such a project. Other individuals have persued these tasks and their work is not covered by this report. Some of the observations made in this report will also no doubt be superseded by additional and more refined studies which are currently in progress. This study is an abstracted summary of a number of SLAC group B internal memos.[2] Material judged to be too detailed or of a background nature, has been omitted. These memos were written during 1969 and 1970 and this report may suffer some in continuity and subject matter because of historical reasons. It should be considered as a reflection of some thoughts in the beginning phase of this project, and not at all as a definite summary.

The function of a vertex spectrometer would be to measure the low momentum particles near the target, such as a recoil proton or a meson(s) in a many particle final state. The problems of designing a multiparticle spectrometer have been discussed in the literature[1] and a variety of spectrometers are being built. For example, the CERN OMEGA system will be using a very large magnet with the target and chambers inside. In contrast the present BNL Lindenbaum spectrometer uses a second low field and large aperture magnet adjacent to one side of the target for the large angle secondaries.

The proposal under study here is to use two magnets. A solenoid with a B field along the beam axis and enclosing the target to measure the slow particles. Fast particles would be transmitted through to a downstream magnet and the second magnet would be a conventional dipole magnet with a magnetic field perpendicular to the beam. For many experiments such a two magnet system would dramatically reduce the aperture demands of a one dipole magnet spectrometer and improve the total as well as angular acceptance.

The solenoid B field (along the Z axis) rotates the P_T (transverse momentum) component of a charged particle inside it. Since the P_T spectrum is relatively invariant over a wide range of energies, reactions and particles,

one can design a solenoid with very universal applications. Thus a large class of experiments could make use of it. As envisaged at SLAC, it would be the front end of a very powerful two-magnet spectrometer system. This is currently being built by group B and is known as "LASS," for Large Aperture Solenoid Spectrometer. It is anticipated to be a general facility for hadron spectroscopy at SLAC.

The proposed SLAC solenoid (2 m × 3 m w/25 kG) should measure those particles with P_L (longitudinal momentum) less than 2 GeV/c very well. Often these are the wide angle low momentum particles that one normally misses with a downstream dipole magnet in high energy experiments.

In the following sections we look at some of the kinematics of high energy reactions and spectrometers. The acceptance, resolution and pattern recognition characteristics are examined in Chapters III, IV, and V respectively. Section II begins with a short introduction to the kinematics of a solenoid magnet.

Very extensive use is made of Monte Carlo simulations and care has been taken to ensure that the particle distributions and kinematics are realistic. By using a spectrometer model and tracking Monte Carlo events through it the questions of acceptance resolution, etc. are easily answered.

In this report, the primary experimental thought is given to the following reactions:

$$\pi p \rightarrow \pi\pi\pi p \qquad \text{(i)}$$

$$Kp \rightarrow K\pi\pi p \qquad \text{(ii)}$$

$$pp \rightarrow p\pi\pi p \qquad \text{(iii)}$$

By detecting and measuring three of the particles ($\pi\pi\pi$ or $K\pi\pi$ or $p\pi\pi$) one can do high statistics meson spectroscopy experiments and or diffractive enhancement studies. The requirement that at least three particles be measured simultaneously is a severe one and it should be representative of difficulties in other many body high energy experiments. The beam momentum ranges in this study from 8 to 16 GeV/c. This approximates the present SLAC beams.

The fact that reaction (i) is used throughout the study should not be interpreted in any way as a limitation on the universality of the solenoid detector. For example, it may be possible to use the solenoid detector as a stand alone

system for missing mass experiments or for K^0 decays. The symmetric ϕ angle acceptance would be useful in the latter. Another real possibility is to study the recoil nucleon resonance states (e.g., $N^*(1400) \rightarrow \Delta\pi$) where all particles may be slow in the lab. But since the meson spectrum must be studied in production experiments, and the nucleon states are seen in detail via formation experiments, the meson kinematics have been emphasized.

Since P_T is measured directly, the solenoid is also ideally suited for studies of this variable. The related topics of inclusive experiments and particle correlations, would also be aided by the large acceptance range of this magnet.

In addition, the unique geometry of the solenoid has made it a prime candidate as a detector for the intersecting beam facility experiments.

II. THE SOLENOID

To a first approximation, all particles produced in strong interactions have a very similar transverse momentum spectrum. The P_T spectrum peaks at about 300 MeV/c and approximately 75% of the particles have $P_T \leq 500$ MeV/c. Figure 1 illustrates one such typical P_T distribution for the pions in 16 GeV/c $\pi p \rightarrow \pi\pi\pi p$ data.[3] This distribution can be parameterized as[4]

$$\frac{dN}{dP_T} \sim P_T^{3/2} e^{-aP_T}$$

The proposal is to use the axial B field of a solenoid to rotate the P_T vector and with the aid of spark chambers to measure the momentum of the particle. These spark chambers would have to be inside the axial B field region to digitize the trajectory. If the beam and B field define the z axis, then the spark chamber intercepts of the charged secondaries will describe a circle in the XY plane. Fitting this circle and knowing B, one can calculate P_T. The P_L value is derived from the ΔZ spacing of the planes. If $P_T \approx 0$ or if P_L is very large the solenoid cannot make a momentum measurement.

Figure 2 sketches the solenoid and a typical trajectory.

In addition to the nice property of measuring P_T directly, the solenoid has other attractive features. One can easily use a target inside the solenoid, since a narrow beam can enter along the central B_Z flux line and thus not be deflected.

The target is assumed to be at the center of the solenoid diameter and inside the upstream end. There may be situations where one would want to change this, but in this report we have not explored these possibilities.

The faster secondary particles are passed through to the downstream magnet and are only rotated by the B_Z field. They will not be deflected into or away from the dipole magnet aperture. The geometrical acceptance angle θ of the bending magnet can still be defined by $\tan\theta = P_T/P_L$ because the solenoid B_Z field does not change the angle θ.

Solenoid Kinematics

A particle of charge q moving through a constant magnetic field B will describe a circular helix. The projected radius of the helix is given by

$$R = \frac{P \cos\lambda_0}{qB} \qquad (1)$$

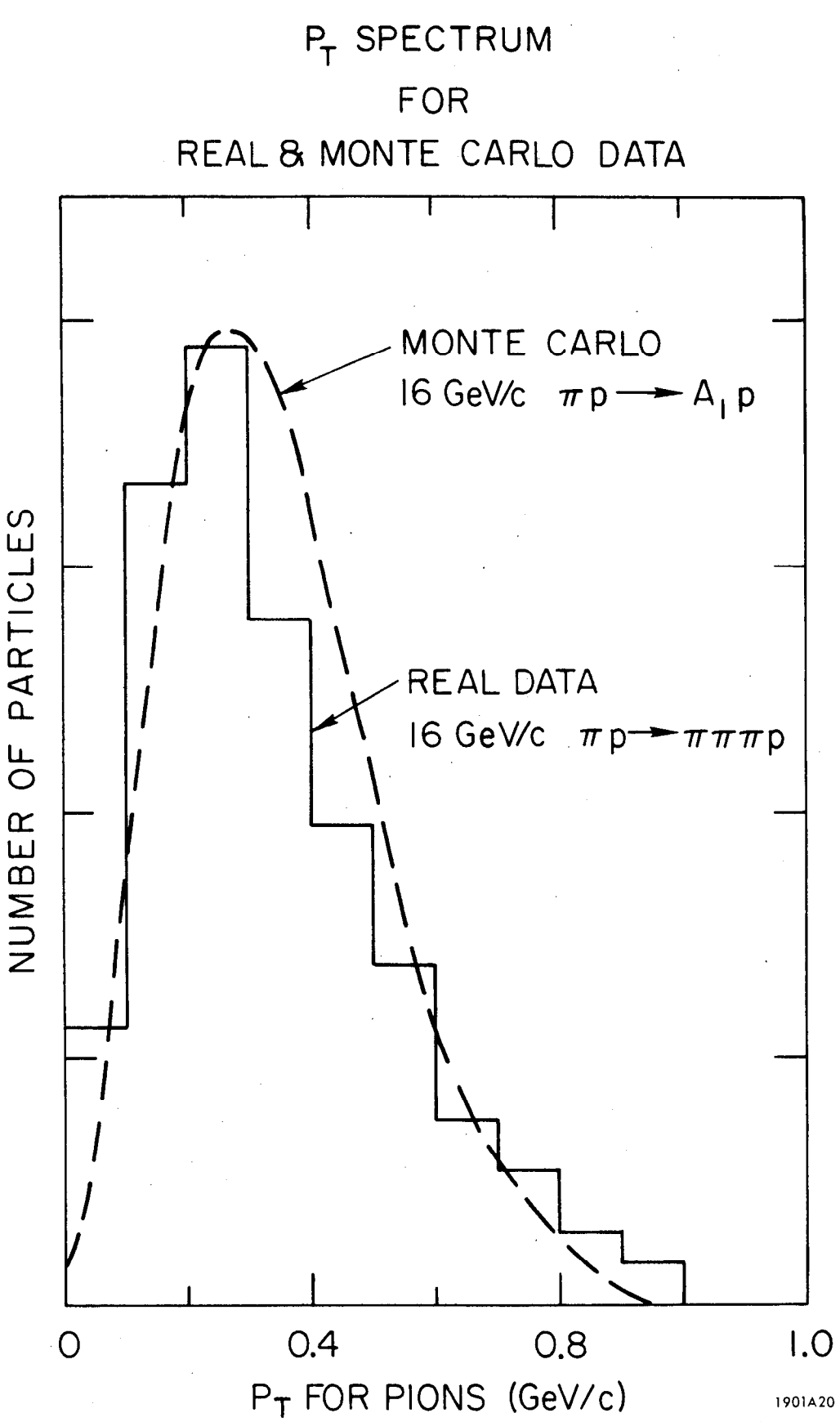

FIG. 1--P_T spectrum for pions in real and Monte Carlo events.

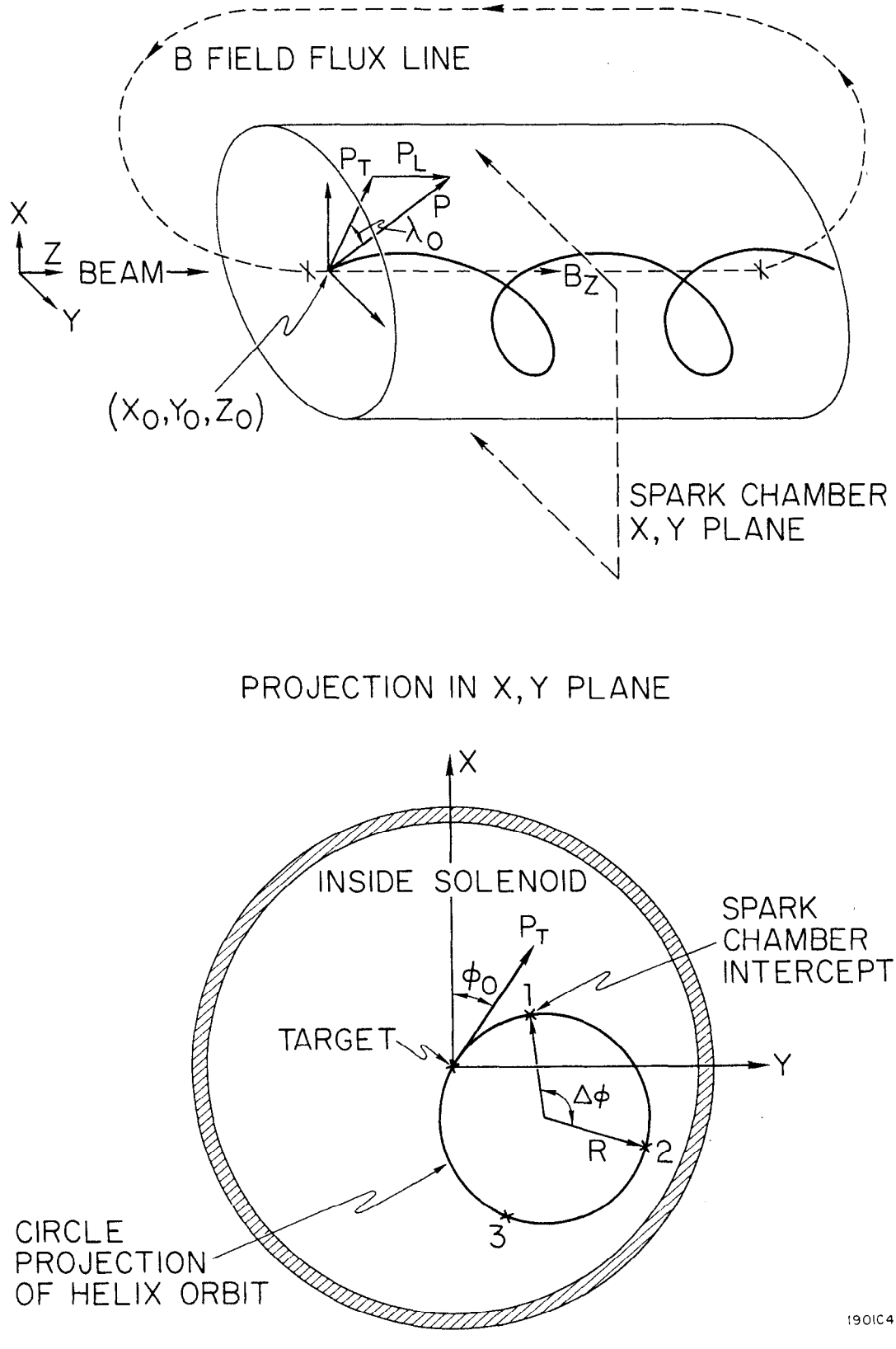

FIG. 2--Sketch of helix trajectory inside a solenoid and its XY plane projection.

and

$$R = 33.36 \frac{P_T}{B} \text{ in meters} \tag{2}$$

where P_T is the transverse momentum in GeV/c, B is the axial field in kG and R is in meters. The angle λ_0 is the helix pitch (or dip) angle.

$$\tan \lambda_0 = \frac{P_L}{P_T}$$

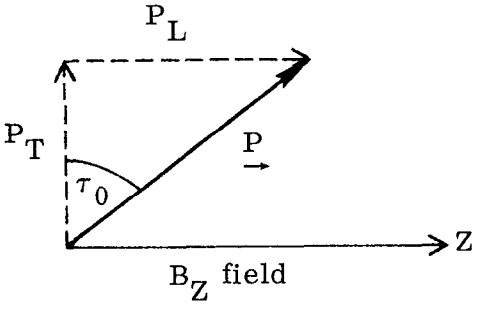

The helix trajectory is described by

$$\Delta Z = Z - Z_0 = \frac{P_L}{m} t = \left(\frac{Pt}{m}\right) \sin \lambda_0 = S \sin \lambda_0 \tag{3}$$

$$\Delta Y = Y - Y_0 = R\left[\cos\left(\phi_0 - \frac{S}{R} \cos \lambda_0\right) - \cos \phi_0\right] \tag{4}$$

$$\Delta X = X - X_0 = -R\left[\sin\left(\phi_0 - \frac{S}{R} \cos \lambda_0\right) - \sin \phi_0\right] \tag{5}$$

$$\phi_0 = \tan^{-1}\left(\frac{P_Y}{P_X}\right)_{Z=Z_0}$$

S is the three-dimensional path length along the helix.

The trajectory describes a cycloid in the r-z plane and has the following equation

$$r = \sqrt{\Delta X^2 + \Delta Y^2}$$
$$r = 2R \sin\left(\frac{\Delta Z}{2R \tan \lambda_0}\right) \tag{6}$$

The maximum displacement of the trajectory from the central beam line is 2R and one complete orbit of the cycloid has

$$\Delta Z = \pi(2R \tan \lambda_0)$$
$$\Delta Z = a_0 P_L \text{ in meters} \tag{7}$$

where P_L is in GeV/c, B in kG and

$$a_0 = \frac{2\pi \times 33.36}{B}$$

For example, if B = 25 kG, P_L = .5 GeV/c, then the full circle orbit would require that ΔZ be approximately 4 meters. Of course one can measure P_T and P_L with a much smaller arc length.

One complete orbit in a 25 kG field and a $\Delta Z \approx 75$ cm (possible chamber spacing) corresponds to $P_L \approx 100$ MeV/c. That is, particles with $P_L > 100$ MeV/c will not make multiple orbits between chamber spaced 75 cm or less.

The $\Delta\phi$ angle subtended by the arc in the xy plane (see Fig. 2) has the simple expression

$$\Delta\phi \text{ (radians)} = \frac{B}{(33.36)} \frac{\Delta Z}{P_L} \tag{8}$$

Figure 3a illustrates this relation between $\Delta\phi$ and P_L for a 25 kG field, and 3b shows how the solenoid diameter varies with P_T. A 25 kG field × 2 meter diameter will "trap" all orbits with $P_T \lesssim 375$ MeV/c. Three XY spark chamber planes spaced 75 cm apart (i.e., total ΔZ = 1.50 m) will subtend an arc of about 60° for a P_L = 1 GeV/c particle.

A more thorough study of acceptance and resolution versus the three basic solenoid parameters (field, diameter and length) is made in the following chapters.

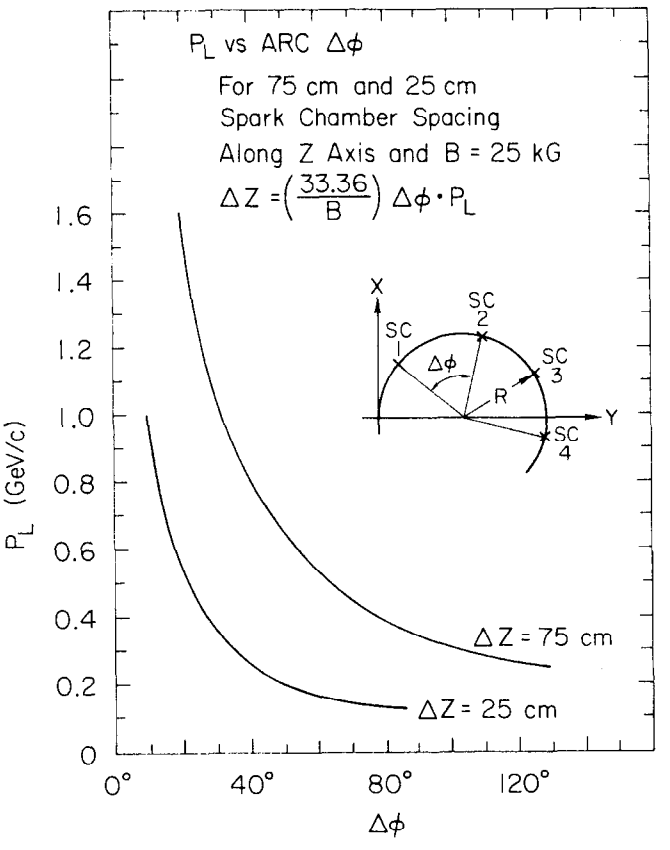

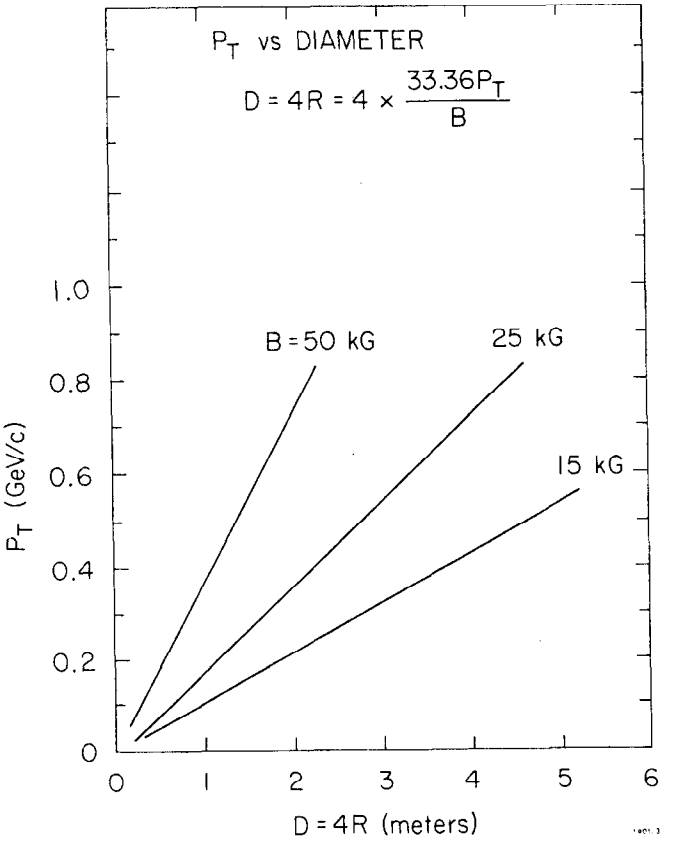

FIG. 3--Solenoid characteristics (a) P_L vs arc $\Delta\phi$ and (b) P_T vs solenoid diameter for a full circle.

III. ACCEPTANCE

A. Gap Magnet Acceptance Difficulties

In the first part of this chapter the acceptance limitations of the one-magnet spectrometer are examined.

The need to measure the momentum of fast particles in counter experiments has led to the development of bending magnet spectrometers. An adequate measurement of the fastest particles means a corresponding lengthening requirement on the fore and aft spark chamber lever arms as well as a large Bdl for the magnet. This in turn can force one to a very large aperture for the gap magnet and downstream chambers. The cost and construction problems grow proportionally.

But, even if one should pursue this line, as soon as one has a many particle (more than one) final state which requires that slow and fast particles be measured simultaneously, new problems arise. For example, the acceptance becomes a strong function of the decay angle of the composite system. Worse still, one is likely to have zero acceptance or dead regions in the very forward-backward decays. This complicates the physics analysis and can made it impossible to answer questions such as "what is the partial wave composition of a mass enhancement?"

1. Model Simulation

A Monte Carlo simulation of a one magnet spectrometer illustrates the point. Figures 4 and 5 sketch the model and the results. In this model the following two reactions are considered.

$$\pi^- p \rightarrow A_1^- p \qquad \text{and} \qquad A_1^- \rightarrow \rho^0 \pi_1^-, \qquad \rho^0 \rightarrow \pi_2^+ \pi_3^- \qquad \text{(i)}$$

$$\pi^- p \rightarrow \rho^0 n \qquad \text{and} \qquad \rho^0 \rightarrow \pi_1^+ \pi_2^- \qquad \text{(ii)}$$

These reactions involve two and three pion final states and are typical of other Kp and pp peripheral interactions. The beam momentum values of 8 and 16 GeV/c are used.

"Events" simulating the above reactions are generated at the point target in Fig. 4 and are traced through the target-gap-magnet regions as shown. The events are basically those of phase space with some modifications to make them more "realistic."

SPECTROMETER MODEL FOR ACCEPTANCE ESTIMATES OF SIMPLE DIPOLE MAGNET

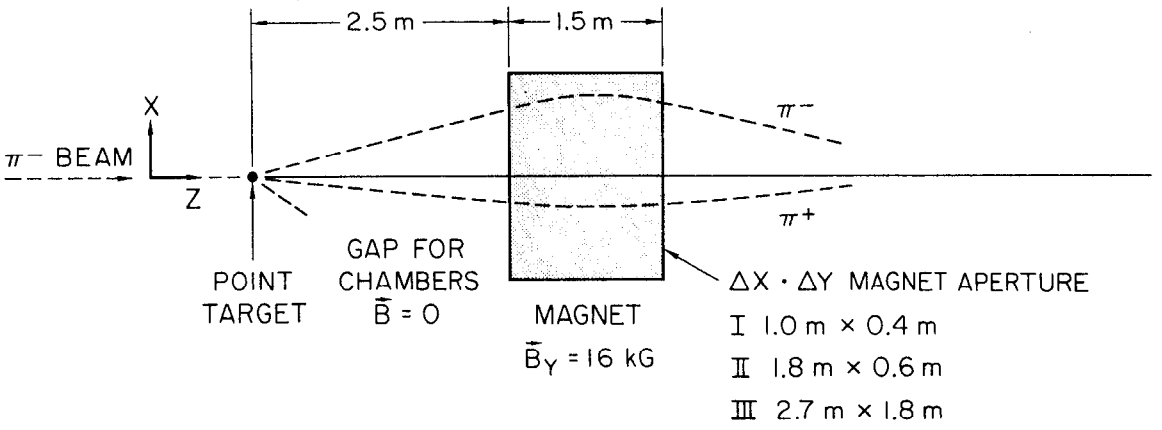

COMPARATIVE EVENT ACCEPTANCES AT MAGNET EXIT

FOR 3π's IN $\pi^- p \rightarrow A_1^- p$

	MAGNET APERTURE SIZE $\Delta X \cdot \Delta Y$		
	I (1.0 × 0.4)	II (1.8 × 0.6)	III (2.7 × 1.8)
8 GeV/c BEAM	0.05%	3%	37%
16 GeV/c BEAM	6%	23%	75%

FOR 2π's IN $\pi^- p \rightarrow \rho^0 n$

	MAGNET APERTURE SIZE $\Delta X \cdot \Delta Y$		
	I (1.0 × 0.4)	II (1.8 × 0.6)	III (2.7 × 1.8)
8 GeV/c BEAM	6%	23%	78%
16 GeV/c BEAM	40%	68%	94%

FIG. 4--Acceptance estimates of a simple dipole magnet spectrometer.

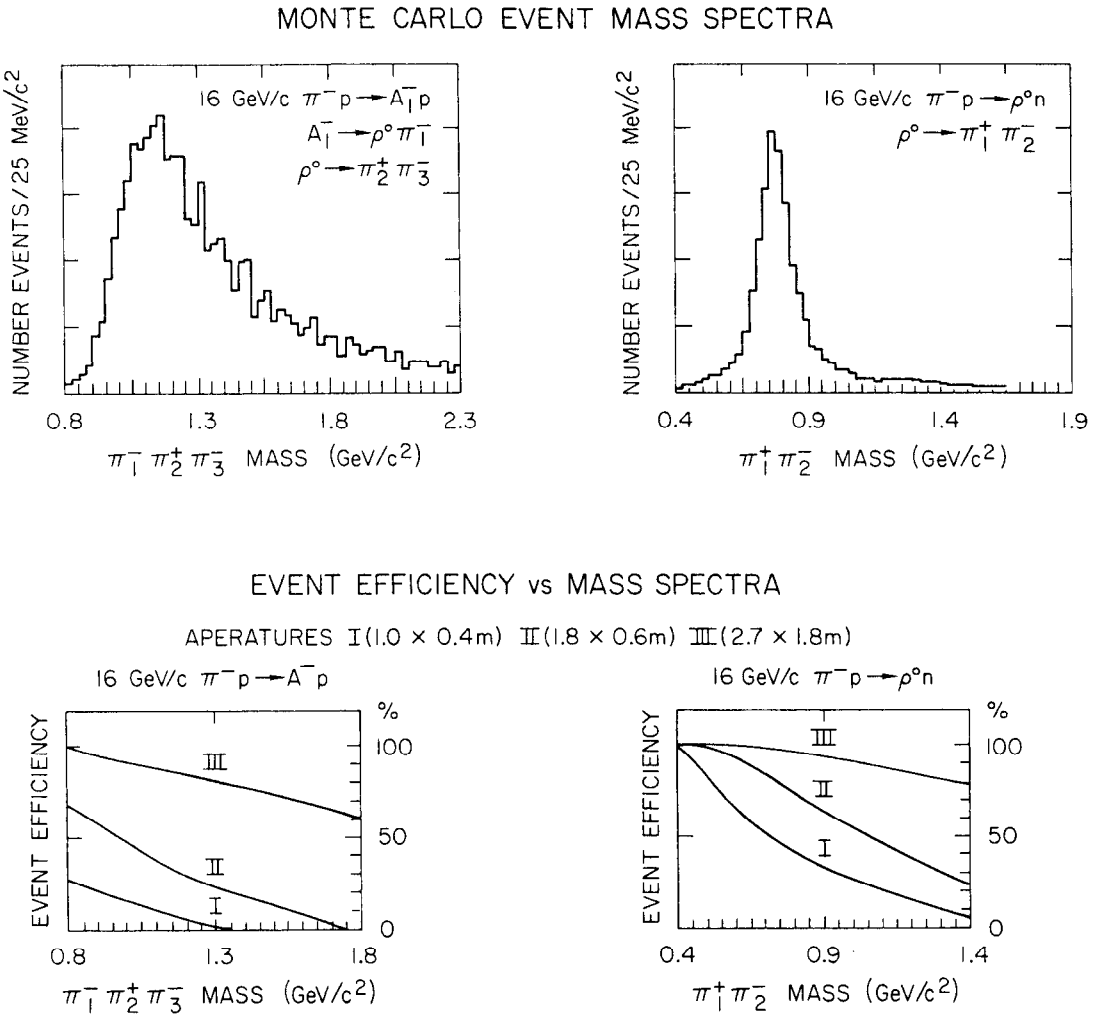

FIG. 5--Event acceptance efficiency as a function of mass and decay angle.

All the ϕ angle decay distributions are isotropic and the cos θ angles for $A_1 \rightarrow \rho\pi$ and $\rho \rightarrow \pi\pi$ are also assumed isotropic. (Real ρ decays, however, have a $\cos^2 \theta$ distribution and our assumption will therefore inflate the total acceptance estimates.)

The following "non-phase-space" modifications are imposed.

(a) The A_1^- resonance in reaction (i) has a Breit-Wigner amplitude with $m_0 = 1050$ MeV/c and $2\Gamma = 200$ MeV/c.

(b) The ρ^0 resonance in reactions (i) and (ii) has a Breit-Wigner amplitude with $m_0 = 765$ MeV/c and $2\Gamma = 125$ MeV/c. Figure 5 illustrates what the respective Monte Carlo event mass spectra look like.

(c) The target nucleon is constrained to be peripheral, i.e.,

$$e^{-At} \times \text{(Phase Space)}$$

where t is the proton $\rightarrow$ nucleon four momentum transfer square and A is set to 8 $(\text{GeV/c})^{-2}$.

The above conditions help simulate real events and so ensure more realistic acceptance estimates. This event generating procedure is used extensively in later studies.[5]

The "point target" is 2.5 meters from the magnet entrance. The magnet is 1.5 meters long and has a "box shape" field of 16 kG over its volume in the Y direction. That is $\int B \cdot dl = 24$ kG-meters in the model.

Only the magnet aperture in the XY plane is varied and the three different sizes are set at

I 1.0 m × .4 m for $\Delta X \cdot \Delta Y$

II 1.8 m × .6 m for $\Delta X \cdot \Delta Y$

III 2.7 m × 1.8 m for $\Delta X \cdot \Delta Y$

Magnet I is of modest size whereas magnet III is quite a goliath.

An event produced at the target is considered as accepted by the system if all its pions π_1^-, π_2^+, π_3^- in reaction (i) and π_1^+, π_2^- in reaction (ii) pass into and through the magnet without striking its walls. No constraint or test is made on the target nucleon. It may be measured but most likely would be detected by a missing mass calculation.

Then, by comparing the target events and the magnet exit events one can give an estimate of total acceptance as well as bin efficiencies for mass, decay angle, proton t distributions, etc.

2. Model Results

It must be emphasized and kept in mind that our spectrometer model is too simple to be a realistic estimate of absolute acceptances for an actual experiment. No account is taken of the nonisotropic ρ^0 decay, the beam plug, target size, spark chamber inefficiencies, losses after the magnet, particle decays, etc. To illustrate, Fig. 4 states that the acceptance for aperture I of 16 GeV/c $\pi^- p \rightarrow \rho^0 n$ is 40%. Group B's experiment E-41 at SLAC, which is somewhat similar to this, found it to be about 6%.

The usefulness of the model is in its qualitative comparison of different apertures, beam energies and final states. The absolute acceptance values at best are only an upper limit.

The table in Fig. 4 summarizes the Monte Carlo event acceptances at the magnet exit for this very simplified spectrometer model.

The table shows magnet III to have a 12 times greater acceptance than magnet I for 16 GeV $\pi^- p \rightarrow A_1 p$ and 74 times greater acceptance at 8 GeV. That is, the aperture size certainly can improve the total acceptance but as we shall see it does not solve all the problems.

Figure 5 illustrates how the acceptance efficiency may vary with the mass or decay angle. One observes that at low invariant mass, where there is little center-of-mass energy in the break up, the efficiencies are high. But they decrease with an increase in effective mass. Aperture I does not accept a 3π mass greater than 1.3 GeV/c^2.

The bottom sketches show that the decay angle efficiencies may have very extreme fluctuations. There are correlations between the efficiencies of cos θ, ϕ, t, $m_{\pi\pi}$, etc., but for ease of presentation these figures show only the efficiency projection on one axis at a time.

The cos θ curves show a maximum efficiency at $\theta = 90^\circ$ and a minimum at $\theta = 0^\circ$. That is, decays transverse to the line-of-flight of the parent particle have a better acceptance than the longitudinal decays. Even for the aperture III curve these $\theta = 0^\circ$ losses are substantial. It is these events that compel one to search for better techniques of measuring the slow and fast pion in the same event.

The ϕ curves are correlated to cos θ and mirror the box shape of the aperture. They do not have a $\pm 180^\circ$ symmetry here because the ϕ angle

refers to only one of the charge pions — and its acceptance is better on the magnet side where it is deflected into the magnet center.

The 8 GeV/c beam momentum curves have not been shown but are similar, with a lower efficiency scale.

In the $A_1^- \to \rho^0 \pi^-$ decay the cos θ = +1 direction corresponds to a forward π^- or backward ρ^0. This backward $\rho^0 \to \pi^+ \pi^-$ usually gives a slow pion which does not make it through the magnet and so the efficiency for these events is very low or zero. The efficiency is changing very rapidly in the +1 region and this can be a very serious problem when one has to reconstruct the real decay distribution.

The "lost" pions in the above extreme decays have typical lab momentum of 250 to 1500 MeV/c and lab production angles of 3^o to 30^o for apertures II and III. Even if these particles make it into the entrance of a large aperture magnet, the low momentum means they will be swept into the magnet walls.

3. Real Data

Since our purpose is to propose a system which will deal with these slow particles let us examine them more closely. We turn to real data[3] and look at

$$16 \text{ GeV/c} \quad \pi^- p \to p \pi^+ \pi_1^- \pi_2^-$$

Figure 6 shows what the P_z momentum component distribution (almost equivalent to P longitudinal) in the lab frame looks like. About 27% of all pions have a $P_z < 1$ GeV/c. For the A_1 mass region it is not quite so high but there are still a fair number less than 2 GeV/c. Obviously, the slow pion problem becomes much more severe at high masses and this will be looked at later in the study. When we refer to "slow particles" in later sections we will imply particles with $P_L \lesssim 2000$ MeV/c.

The proposed solenoid plus gap magnet system which we shall examine in some detail, offers a very promising solution to this "slow particle problem."

B. Solenoid System Acceptance Studies

To study what the particle acceptance characteristics would be for a solenoid and dipole magnet spectrometer system, we again turn to a Monte

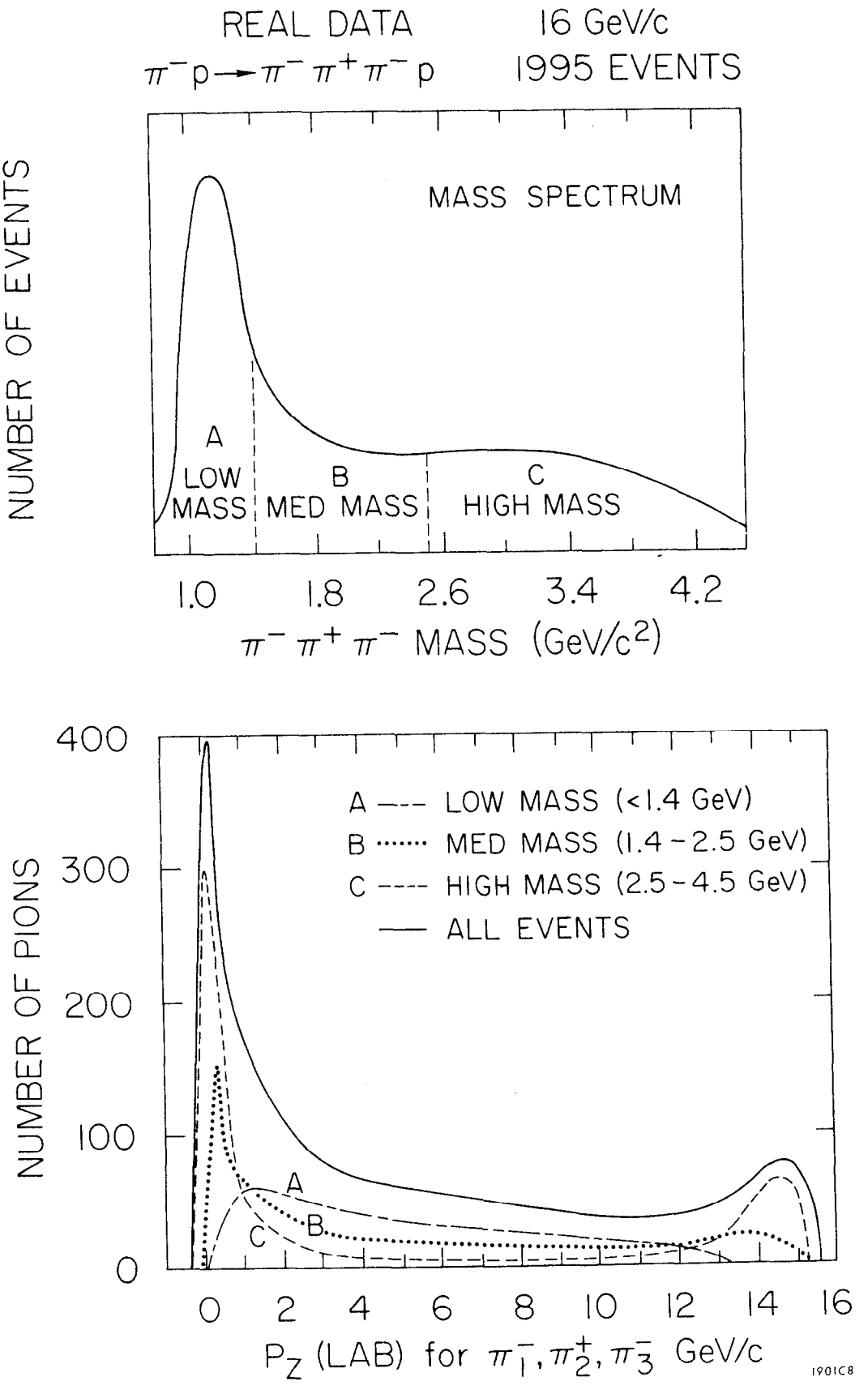

FIG. 6--P_Z distribution of pions for real 16 GeV/c data.

Carlo model. The specific aim is to study the

1. absolute acceptance,
2. limiting aperture and
3. decay angle efficiencies

when the spectrometer parameters are varied. From this one can minimize the solenoid-magnet size yet maintain acceptable efficiencies and have a reasonable match of the several spectrometer apertures.

1. Introduction

The sketch in Fig. 7 illustrates the spectrometer model used in the present study.

The magnets were assumed to have perfect "box" shape fields. The fringe field problem is not examined in this report.

Given the above geometry and a Monte Carlo event originating from the target, all the charged particles of interest are traced through the solenoid, first gap, magnet, and second gap. Checks are then made to see if all the particles of interest in the event would pass through the geometrical apertures to the last spark chamber plane. A test is also made on the tracks which failed to get through all apertures to see if an acceptable measurement could have been made by the solenoid.

Knowing the number and type of events generated, one can study the acceptance numbers as well as biases from the events which had all their tracks measured by the gap magnet or solenoid.

The acceptance and bias depends on a large number of parameters. In this note we hope to get a quantitative estimate on the important ones.

The parameters are

(a) the interaction or final state
(b) the beam momentum
(c) the target dimensions
(d) the solenoid length ΔZ_s
(e) the solenoid radius r
(f) the solenoid field strength B_z
(g) the solenoid measurement acceptance in $\Delta P/P$

} Solenoid

(h) the first gap length Δz
(i) the beam "plug" size

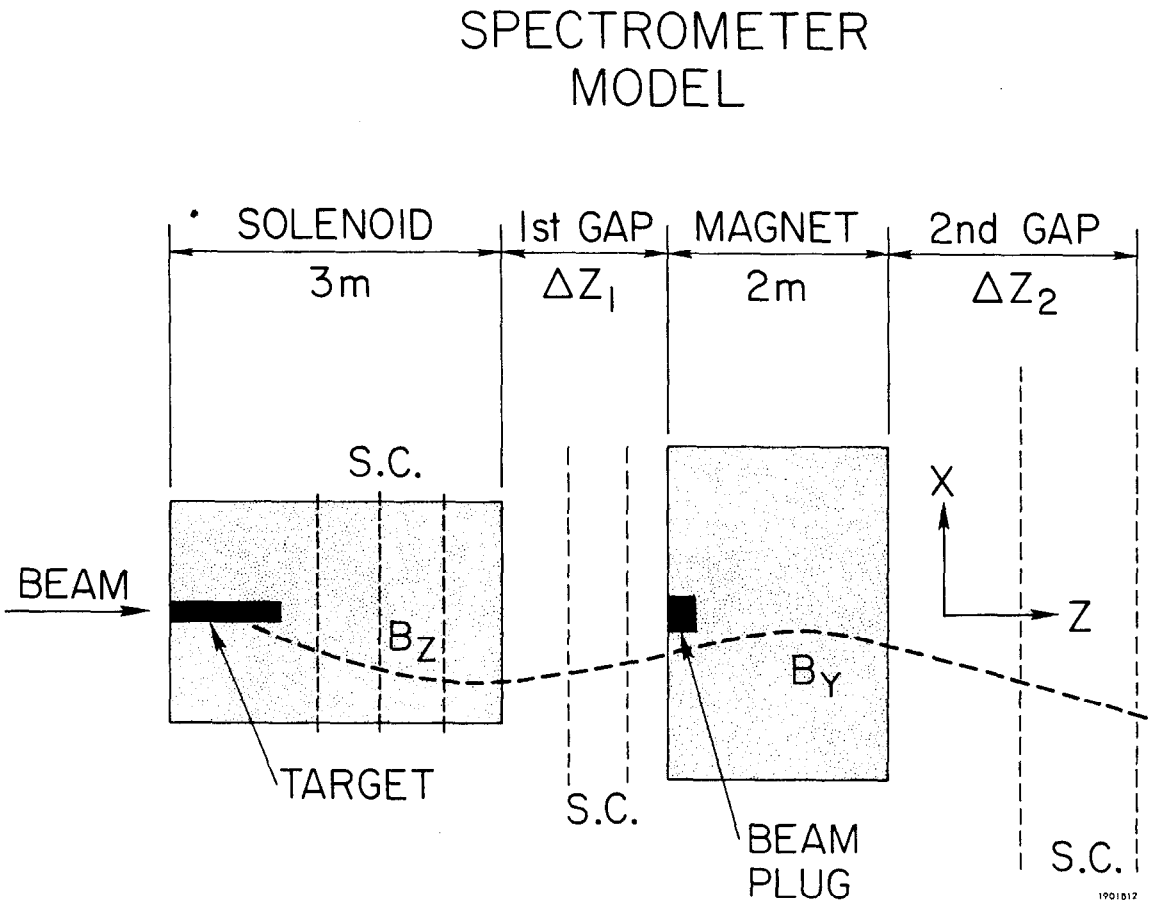

FIG. 7--Sketch of solenoid plus gap magnet spectrometer model.

(j) the gap magnet length ΔZ_M
(k) the gap magnet aperture $\pm\Delta X$ and $\pm\Delta Y$ } Dipole
(l) the gap magnet field strength B_Y
(m) the second gap length ΔZ_2
(n) the second gap aperture $\pm\Delta X$ and $\pm\Delta Y$

Not all of the above parameters are given equal weight. One cannot hope to minimize the cost and build a completely general system for all reactions at all energies. In addition, the computer time and study time become prohibitive if one is to exhaust all the parameters.

2. Parameter Comments

(a) Final state

The reaction used to test the acceptance is

$$\pi^+ p \rightarrow \pi^+\pi^-\pi^+ p$$

Nothing is done with the proton and an "accepted" event is defined as one where all three pions could be measured. The analogous Kp and pp reactions would have similar criteria.

Two separate studies are considered. First, a detailed look when the three pions come from an $A_1 \rightarrow \rho\pi$ and $\rho \rightarrow \pi\pi$ cascade reaction and so $m(\pi\pi\pi)$ is in the 1 - 1.5 GeV/c^2 mass region. This is called the "low mass" study. Secondly, we remove the intermediate Breit-Wigner constraints and look at the higher mass events.

In every case, care was taken to be sure that the Monte Carlo events simulated the real world.

Particular attention was given to the P_T distributions. The SLAC 16 GeV/c data $\pi p \rightarrow \pi\pi\pi p$ was used for comparisons.

(b) Beam momentum

The π^+ beam momentum was varied from 8 to 20 GeV/c (the present SLAC range). It turns out that the 3 pion acceptance problems at 8 GeV/c are mostly in aperture size but at 16 GeV/c the beam plug losses become substantial. Most of the study was done at 16 GeV/c.

(c) Target

The target dimensions are fixed at 4 cm × 4 cm × 50 cm in total length for ΔX, ΔY, ΔZ. The target is inside the solenoid and centered along its

Z axis. The vertex or reaction origin is picked at random in this volume. A small pencil target and possibly the track pattern recognition will improve the acceptance.

(d) Solenoid ΔZ

The solenoid length was fixed at 3 meters. This allows for 3 or 4 spark chamber planes inside it. The solenoid momentum resolution goes as $(P_L/\Delta Z)^2$. That is, if one wishes to measure higher momentum tracks in the solenoid, the length should be increased.

(e) Solenoid r

The solenoid radius was examined at r = .5 m, .6 m, .75 m, and 1.0 m. The solenoid event acceptance depends on this radius, but also and more important, on the beam momentum (at low invariant mass). For example, at 8 GeV/c and masses < 1.5 GeV, only in 29% of the events do the 3 pions exit from the solenoid if r = .5 m. At 20 GeV/c this is 80 percent.

Most of the study was done with r = 75 cm and r = 100 cm. This approximate aperture size seems practical and collects sufficient low momentum tracks from 8 to 20 GeV/c. If the B_Z field of 25 kG is not used, an aperture change should also be considered.

(f) Solenoid B_Z

The nominal B_Z = 25 kG was used as the proposed value. B_Z = 15 kG and 50 kG are also examined.

(g) Solenoid $\Delta P/P$

For each track which does not pass through the gap magnet and its spark chambers, a check is made to see how accurately the solenoid could have measured it. (A detailed resolution study is done in the next chapter and the following equations are discussed there.)

$$\frac{\Delta P}{P} \propto \frac{\Delta S}{B_Z} \frac{P_L^2}{P_T \Delta Z^2}$$

and assuming $\Delta S = \pm .5$ mm for the spark accuracy we get

$$\frac{\Delta P}{P} \text{ (in \%)} \approx .01625 \frac{P_L^2}{B_Z P_T \Delta Z^2}$$

(with P_L and P_T in MeV/c, B_Z in kG and ΔZ in meters).

One then defines a particle as measurable in the solenoid if

(1) it exits through the solenoid and

(2) $\Delta P/P < N\%$.

Most of the results shown here set N= 1%. That is, we require that the solenoid measure the momentum to within 1%. (Some cases with N= 5%, 3%, 3/4%, and 1/2% were studied.)

(h) First gap ΔZ

The gap between the solenoid and the gap magnet is intended for possible spark chambers. The gap length was set at ΔZ = 1 meter or at ΔZ = 2 meters. The longer this gap, the larger the gap magnet aperture must be to accept the same number of diverging track trajectories. The ΔX and ΔY aperture limits are set equal to the opening in the gap magnet and thus the "GAP" losses are really due to the $\Delta X \cdot \Delta Y$ size of the entrance to the magnet.

(i) Beam plug $\Delta\theta$

It is assumed that the π^+ beam trajectory must have a "plug" through the gap magnet. This dead region is here defined as a $\pm\Delta\theta$ cone centered on each beam track. $\Delta\theta = \tan^{-1}(P_T/P_L)$ by definition. A $\Delta\theta$ = 30 milliradians was the nominal setting. This corresponds to ±12 cm at a distance of 4 meters from the target and is a liberal estimate for our 4 × 4 cm target. A $\Delta\theta$ = 0, 15, and 50 milliradians was tried. This "plug" was assumed to be located at the entrance of the gap magnet.

The A_1 decay events with a track hitting this plug are substantial at 16 GeV/c and cause decay efficiency losses in preferred directions. (The forward cone nature of very high energy reactions is illustrated by the fact that at 60 GeV/c for example, 80% of the A_1 type of events are lost in a $\Delta\theta$ = 30 mrad plug.)

The one π^- track was assumed to be always separable from the beam cone. In the high mass study this beam plug constraint was removed.

(j) Magnet ΔZ

The magnet length was fixed at 2 meters.

(k) Magnet aperture ΔX and ΔY

One of the primary objectives of this chapter was to see what the large magnet aperture would have to be to match it with the measuring power of the solenoid.

Therefore the acceptance (i.e., percentage loss) tables show three magnet aperture sets. They are:

$$\pm \Delta X \cdot \pm \Delta Y = 1.0 \times 0.5 \text{ m}$$
$$\pm \Delta X \cdot \pm \Delta Y = 1.0 \times 1.0 \text{ m}$$
$$\pm \Delta X \cdot \pm \Delta Y = 1.5 \times 1.0 \text{ m}$$

By looking at the event losses as a function of aperture size and in particular at the fraction lost in the lst gap or magnet aperture one directly sees how the magnet matches the solenoid and plug losses.

(l) Magnet B_Y

The gap magnet B field was set to 15 kG and a check made to see what effect 20 kG would have. Since $\Delta Z = 2$ m, the $B \cdot \ell \equiv 30$ kG-m for most of the study.

(m) Second gap ΔZ

The second gap length, from the magnet to the last spark chamber was fixed at 4 meters for the A_1 study and 3 meters for the high mass events.

(n) Second gap ΔX, ΔY

This constitutes the last aperture of the system and it was set at $\pm 2.5 \times \pm 2.0$ meters, except for one run where it was varied from 2×1 to 4×3.

3. Solenoid Geometry and Acceptance

Solenoid geometry

The solenoid's purpose is to analyze the "low" momentum particles. Its acceptance, however, at low momentum, is very sensitive to the P_T vs P_L spectrum of the particles, the field B_Z and aperture r of the solenoid.

Figure 8 illustrates this point. It shows the P_T vs P_L loss-acceptance boundary for several solenoid geometries. This curve follows from

$$r = 66.72 \left(\frac{P_T}{B}\right) \sin\left(\frac{\Delta Z}{66.72} \frac{B}{P_L}\right)$$

where r is the radius of the particle's trajectory inside the solenoid, measured from the origin on the beam axis. P_T and P_L are the particles' transverse and longitudinal momenta, B and ΔZ are the field and solenoid length.

Figure 8 shows that a 50 kG solenoid has the very ideal characteristic of trapping almost every particle (with $P < 525$ MeV/c) whereas a 25 kG solenoid will lose particles with $P_T > 300$ MeV/c and $P_L < 1500$ MeV/c.

This figure also emphasizes the importance of having a very "realistic" P_T vs P_L spectrum in the Monte Carlo events for an evaluation of the solenoid.

Figure 9 shows the r spectrum of the Monte Carlo events used in our analysis for 8 and 16 GeV/c, $\pi p \rightarrow Ap$. It is this spectrum which determines the solenoid losses. We have defined a "loss" here as the case when the particle does not get through all chambers. In practice one may be able to relax this.

It follows that at lower beam values, and higher masses, the solenoid field B_Z and aperture size become more critical because of the lower P_L spectrum of the particles. For a "totally" trapping solenoid (e.g., 50 kG and R = 1 m) there would be very little acceptance variation with beam momentum.

A solenoid with $B_Z = 25$ kG, diameter $D = 2R = 2.0$ meters and length $\Delta Z = 3$ meters is observed to have fairly good acceptance as well as $\Delta P/P$ resolution for the Monte Carlo samples studied.

The $\Delta^2(P \rightarrow P)$ efficiency is also reasonable out to 0.6 $(GeV/c)^2$ at 16 GeV/c. The acceptance is dropping and about 10% at 0.6. The larger Δ^2 were not examined in this study. Figure 15 illustrates the efficiency vs Δ^2. One should remember that the $\Delta^2 = 0$ region would have losses due to a beam plug (Fig. 15 assumes no plug).

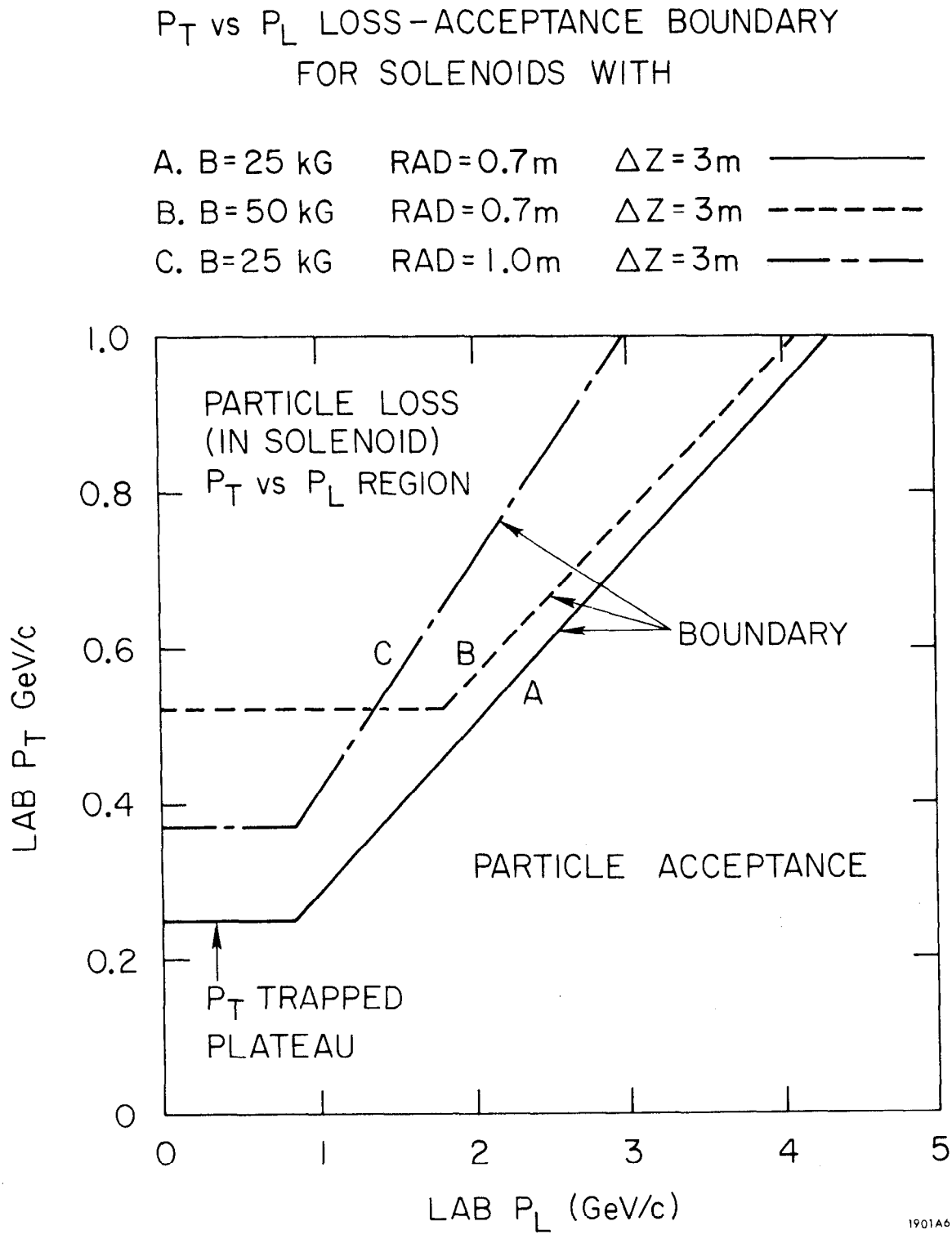

FIG. 8--Particle acceptance (and loss) inside the solenoid as a function of its P_T, P_L and the solenoid parameters.

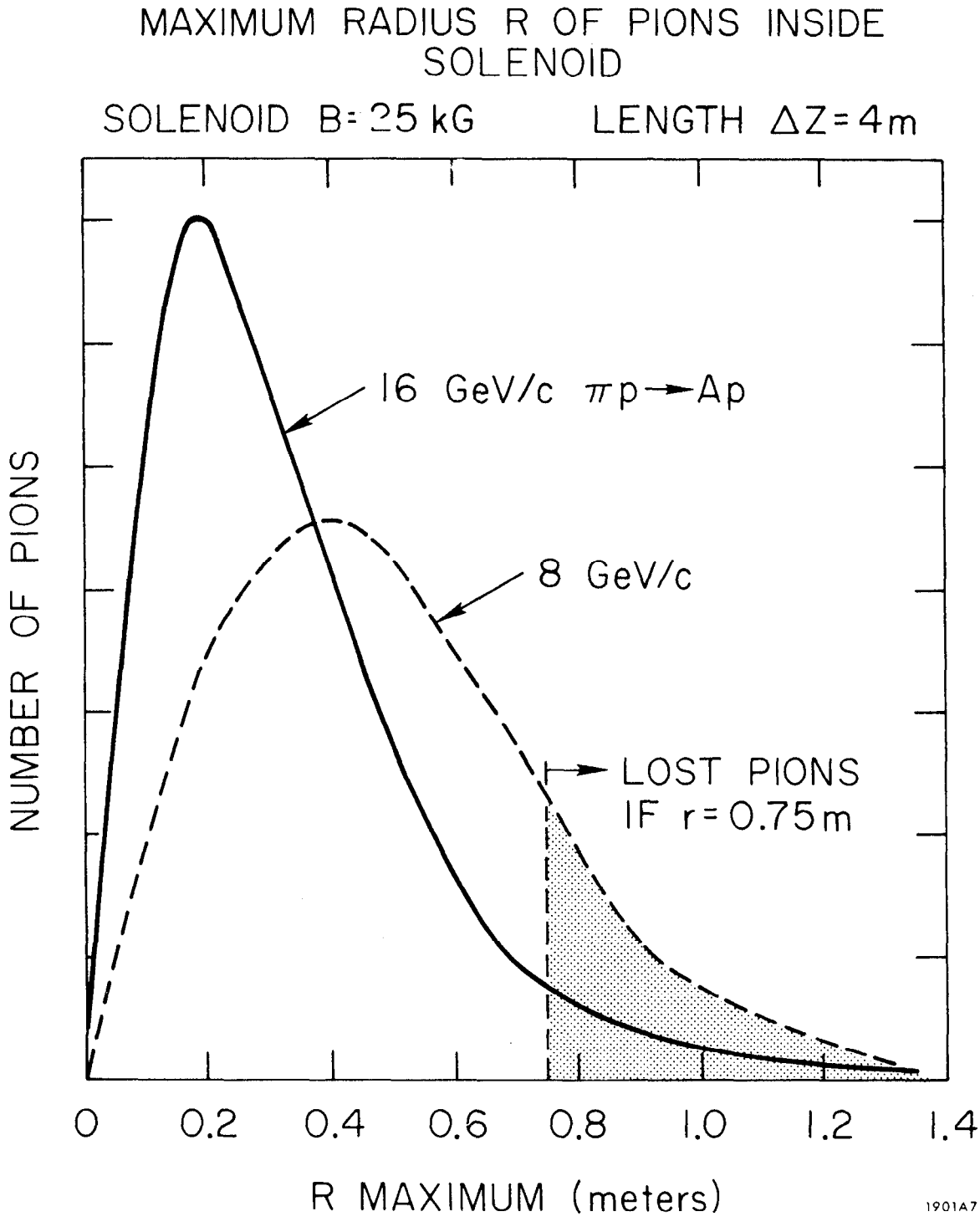

FIG. 9--A typical distribution of maximum pion radius inside the solenoid, from pions in $\pi p \rightarrow \pi\pi\pi p$ (A_1 region).

4. Decay Efficiencies

Besides improving the total event acceptance of the system, the solenoid also plays the very important role of filling in "dead regions" for the decay distributions.

Figure 13 illustrates how the "with solenoid" system fills in the $\cos\theta = \pm 1$ region. This should make spin parity and partial wave decompositions much easier.

Figure 14 shows the mass dependence of the $\cos\theta$ curves. The event totals used were small and one should not take the detail shapes very seriously. The important point is that it be nonzero throughout, even at high masses.

C. Low Mass Acceptance ($m(\pi\pi\pi) < 1.5$ GeV/c^2)

1. Solenoid $\Delta P/P$ Resolution

Due to the large number of low momentum particles, the number of particles versus solenoid $\Delta P/P$ resolution spectrum appears as shown in Fig. 10b. There are more particles from 0 - 1% than from 1 - 2%, and so on from 2 - 3%, etc.

In Fig. 10a one sees the lab momentum spectrum of those pions which do not make it through the gap magnet system and so must be measured in the solenoid. The < 1% spectrum does not go much past 2 GeV/c and thus these particles should be measurable with $\Delta P < \pm 20$ MeV/c in the solenoid.

2. Solenoid P_T Rotation

Because of our perfect axial B field assumption, the θ angle, defined by $\tan\theta = P_T/P_L$ is not at all affected in our solenoid field model. The fringe field B_r component will disturb the P_T/P_L ratio and should be considered.

The azimuthal angle ϕ, defined by $\tan\phi = P_Y/P_X$ will be changed by the solenoid. Figure 11 illustrates the $\Delta\phi$ spectrum. That is, even the fast tracks will experience a $\Delta\phi$ rotation of the order of $5 - 40^{\circ}$.

3. First Gap Length

The solenoid-magnet gap length should be 1 to 2 meters long if we are using the "small" magnet. The intermediate and large magnet are more tolerant and a 3-meter (or larger) gap length could be acceptable.

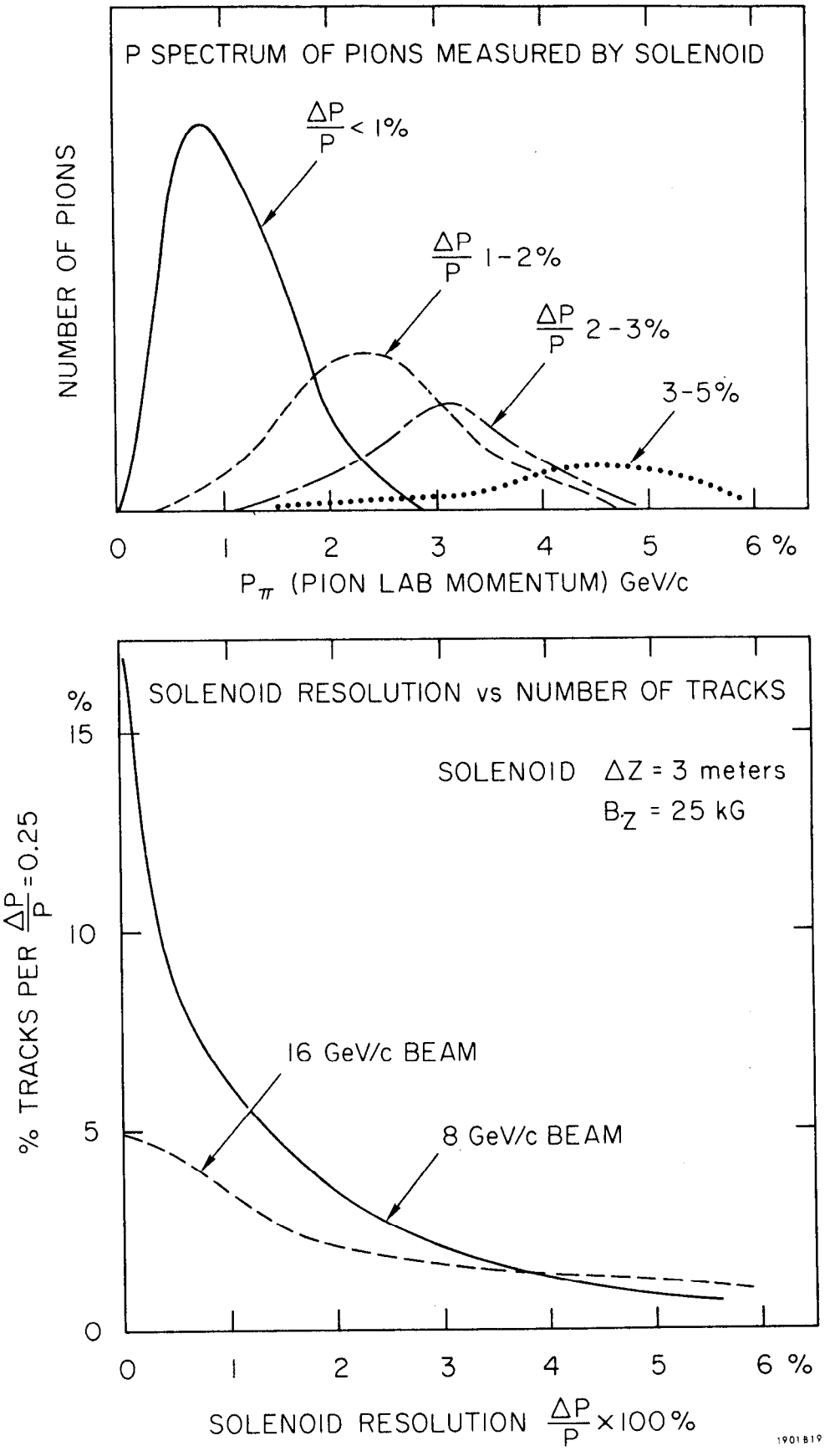

FIG. 10--Pion momentum resolution (A_1 region) studies vs the number of pions and their momentum.

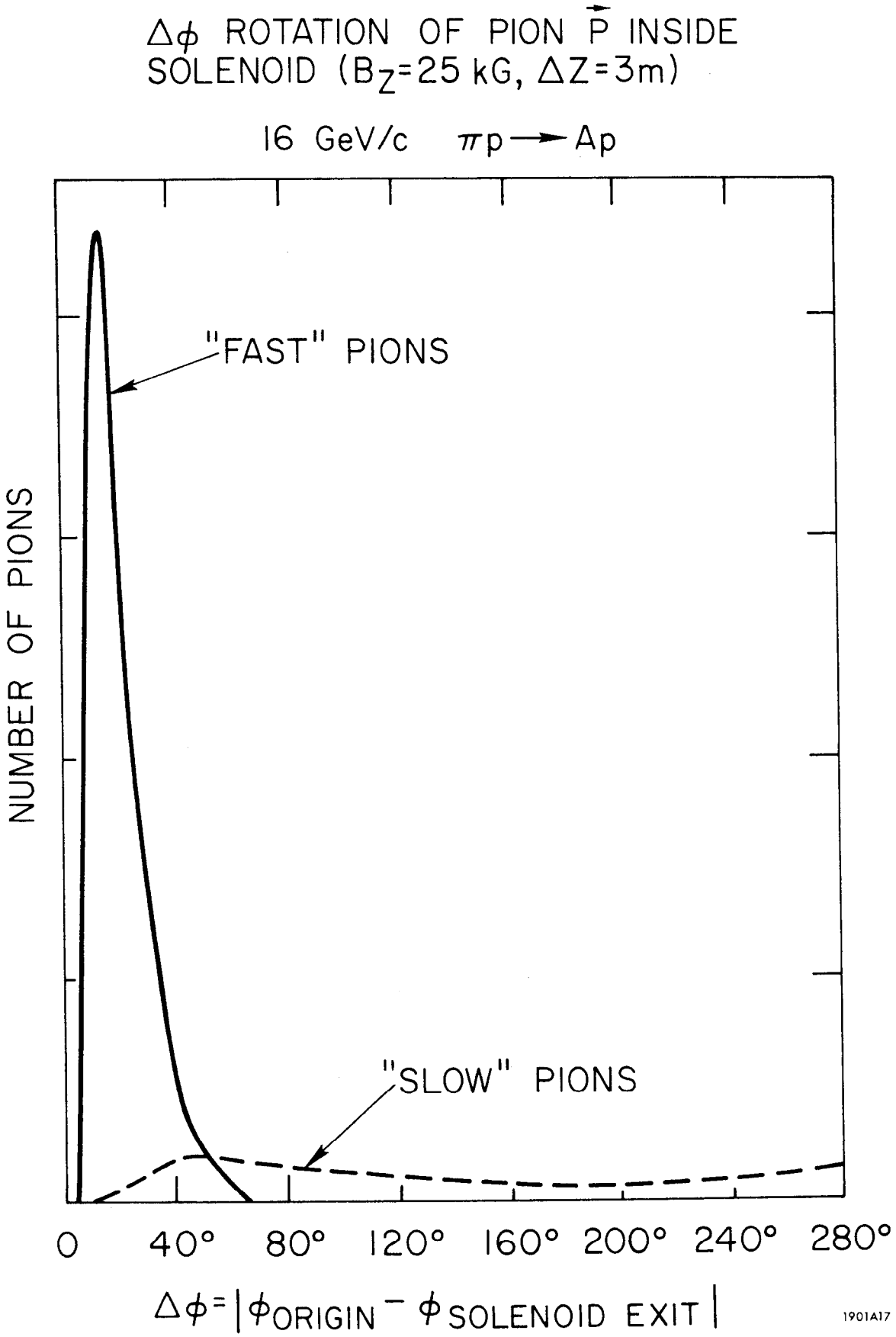

FIG. 11--Typical distributions of ϕ rotation inside the solenoid (A_1 region).

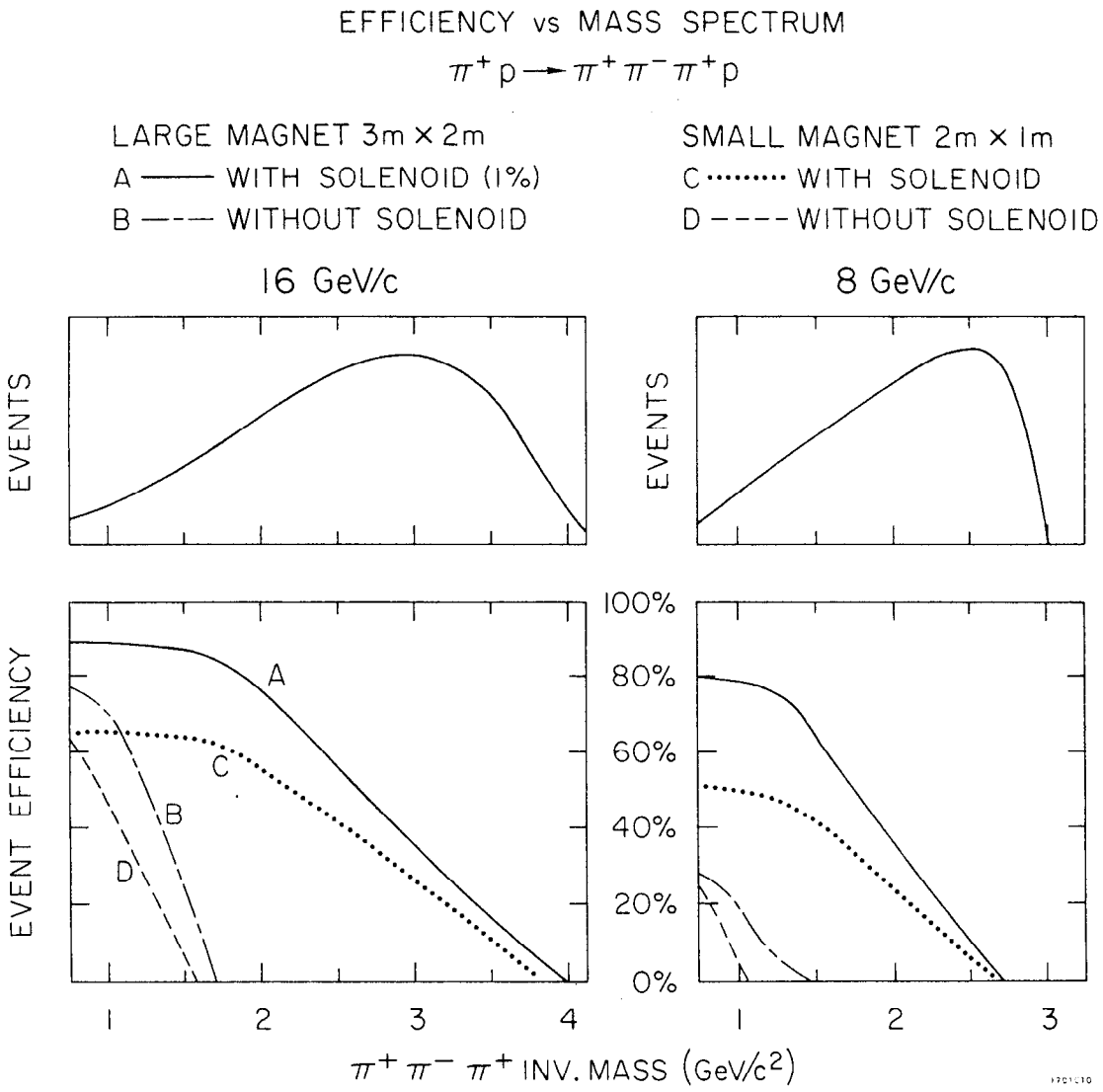

FIG. 12--Acceptance efficiency vs the three pion mass (up to 4 GeV/c) and a comparison with the no solenoid system. Also shown are its variation with beam momentum and gap magnet size.

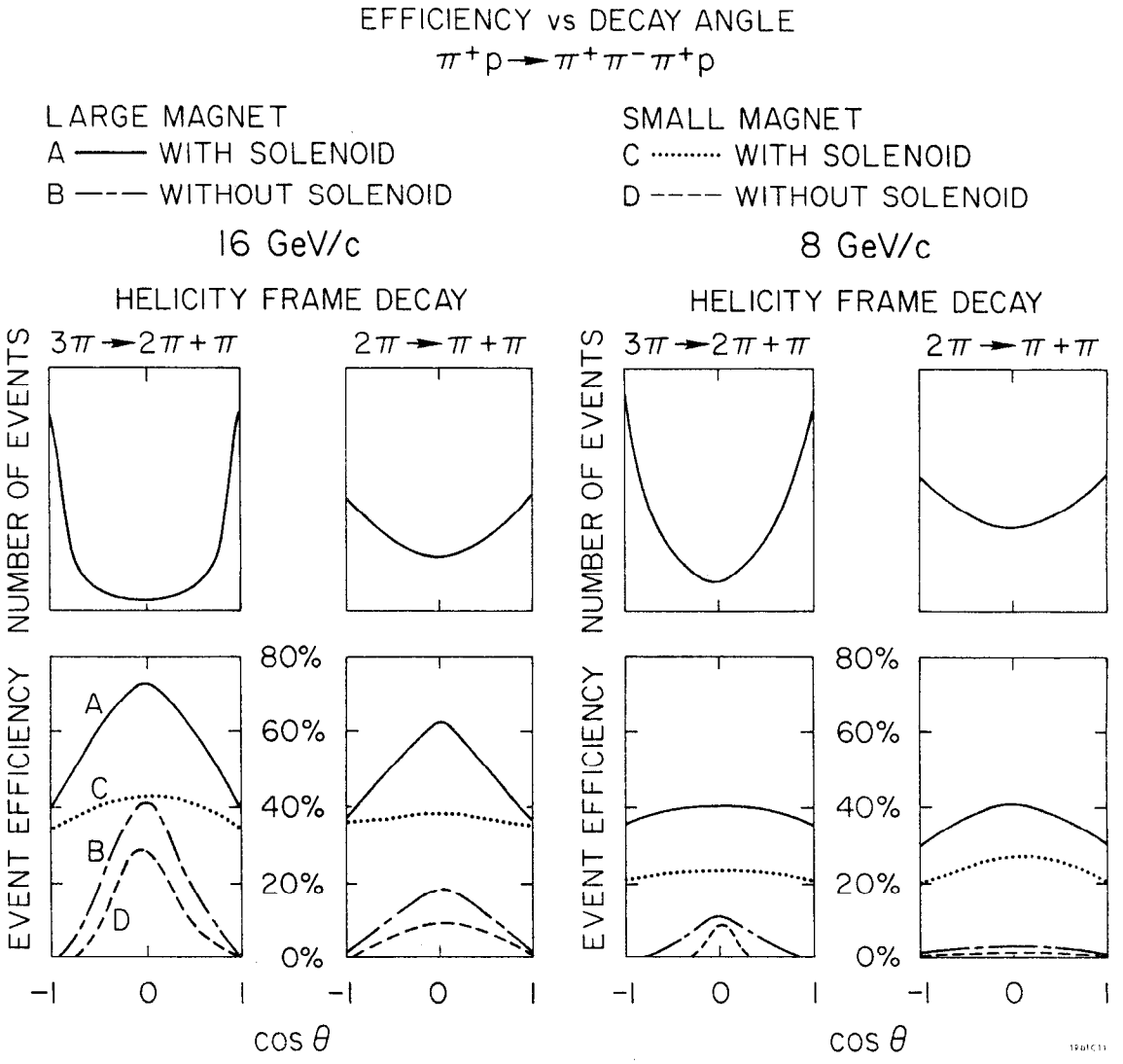

FIG. 13--Same as Fig. 12 but with acceptance efficiency vs the decay angle cos θ.

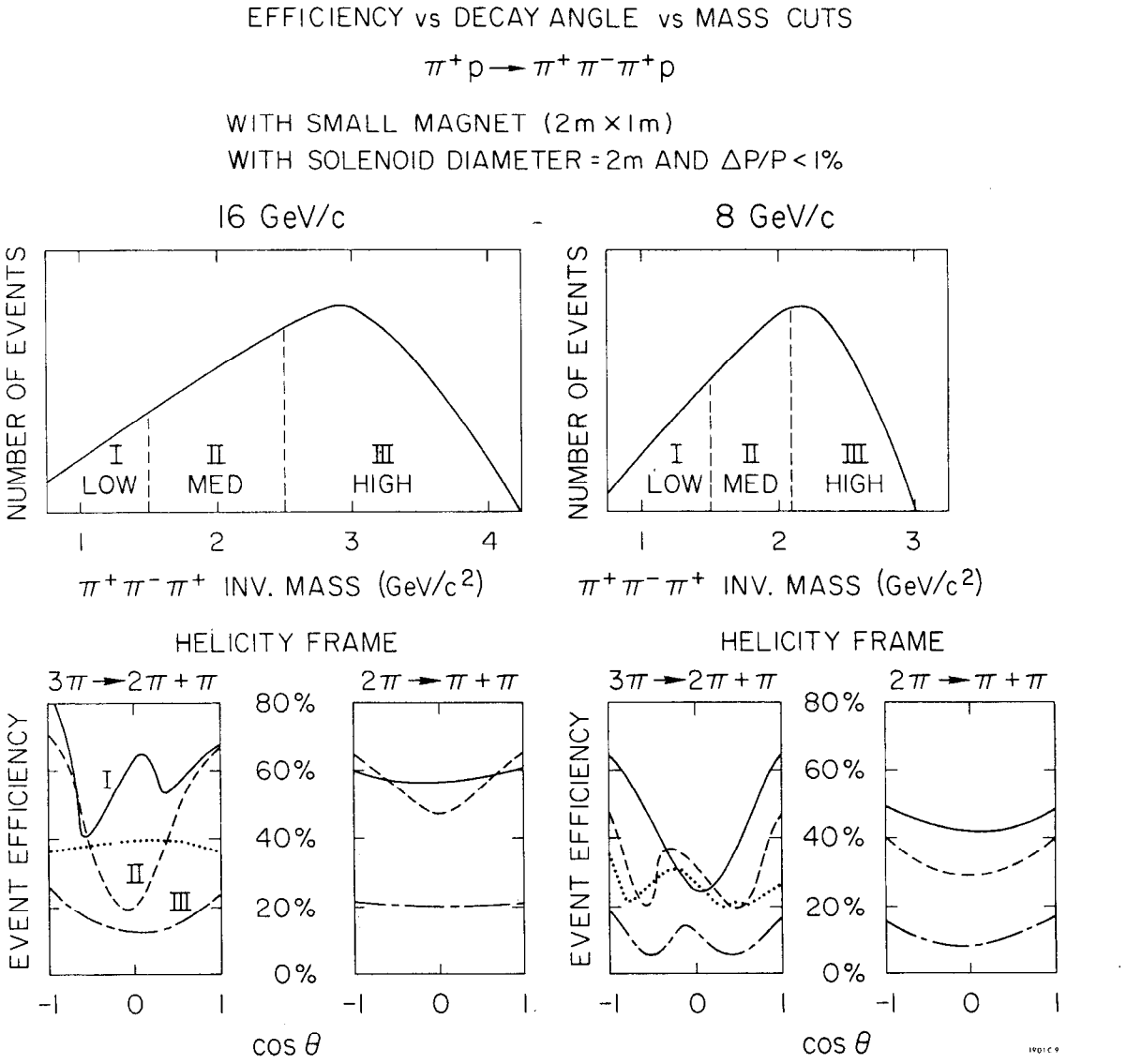

FIG. 14--Same as Fig. 12 but with mass cuts.

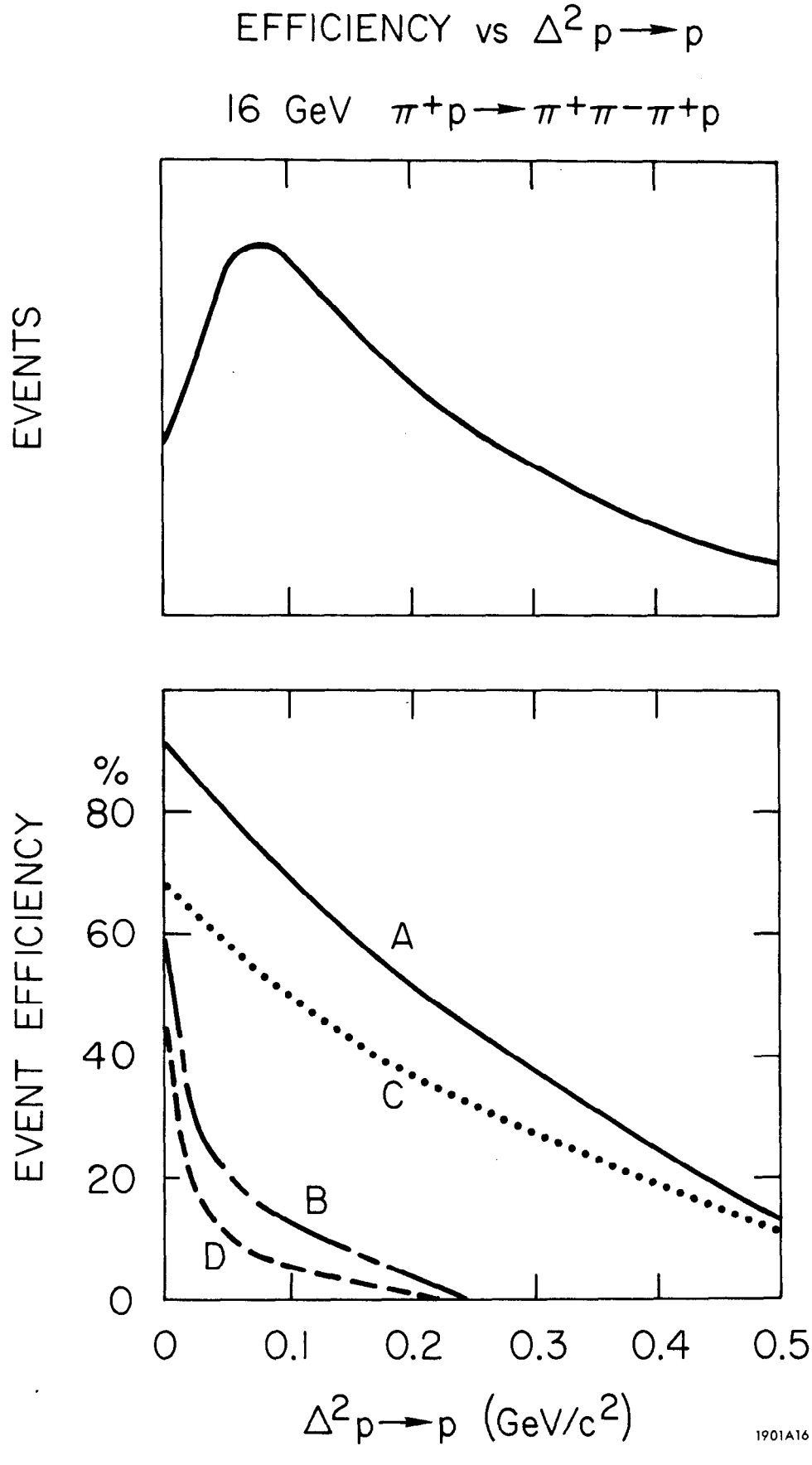

FIG. 15--Acceptance efficiency versus the peripheral proton four momentum transfer.

At 8 GeV/c the loss in the first gap will vary from 1/2% to 40% depending on the ΔX, ΔY, and ΔZ dimensions. At 16 GeV/c the same losses range from 1/2% to 27%. These numbers are found in Table I.

However, whether the loss is 1/2% or 40% the decay cos θ distributions for the events measured by the solenoid-magnet system is still good.

4. Magnet Aperture

Table I shows the following gross characteristics.

(a) A 3 m × 2 m magnet has almost the acceptance of a 2 m × 2 m magnet. The larger magnet acceptance may be improved by about 5% if one uses larger back chambers.

(b) The 2 m × 1 m magnet acceptance is about 15% lower than for the above larger magnets. It still has a respectable 30 - 45% acceptance.

Lines 17 - 20 in the table demonstrate how acceptance and losses fluctuate with magnet changes. The magnet loss increases by about 5% as B_Y is raised from 15 to 20 kG. The geometrical losses of $\Delta Y = 2\ m \rightarrow 1\ m$ are seen to be much more drastic than the small sweeping loss change in $\Delta X = 3\ m \rightarrow 2\ m$.

5. Plug Losses

The 30 mrad beam plug causes a 21% acceptance loss. If there was no plug, the solenoid-large magnet system would have an acceptance increase of 17%. That is, almost all of the "plug" losses are measurable events.

This is not quite the case for the no-solenoid system. About half the events with a very fast track also have a slow track which then is missed.

6. No-Solenoid System

Table II shows that the event acceptance is reduced by about a factor of two at 16 GeV/c when one takes out the solenoid magnet. At 8 GeV/c the reduction is a factor of 10 or worse.

The conclusion is that without the solenoid, and even with a large magnet, at 8 GeV/c the three-pion acceptance is very small (about 5%). With the small magnet it is essentially zero.

TABLE I

ABSTRACTED SUMMARY OF ACCEPTANCES FOR SOLENOID MAGNET SYSTEM

Mass ($\pi\pi\pi$) < 1.6 GeV

System Parameters	A. "Small" Magnet Aperture $\pm\Delta X \cdot \Delta Y = \pm 1$ m $\cdot$ 1/2 m.						B. "Medium" Magnet Aperture $\pm\Delta X \cdot \Delta Y = \pm 1$ m $\cdot$ 1 m.						C. "Large" Magnet Aperture $\pm\Delta X \cdot \Delta Y = \pm 1\frac{1}{2}$ m $\cdot$ 1 m.					
	% Acceptance	Percentage Losses in					% Acceptance	Percentage Losses in					% Acceptance	Percentage Losses in				
		Sol.	Gap 1	Plug	Mag	Gap 2		Sol.	Gap 1	Plug	Mag	Gap 2		Sol.	Gap 1	Plug	Mag	Gap 2
1. 16 GeV: B_Z = 25 kG, r = 75 cm $\Delta P/P < 1\%$, ΔZ_1 = 1 m, $\Delta\theta$ = 30 mrad, B_Y = 15 kG	36%	9%	13%	17%	22%	4%	52%	9%	--	21%	10%	7%	53%	9%	--	21%	4%	13%
Changes from 1																		
2. 8 GeV/c beam	27%	25%	24%	3%	20%	1%	45%	25%	--	5%	20%	5%	45%	25%	--	5%	14%	11%
3. 12 GeV/c beam	33%	13	17	10	25	2	54%	13	--	13	13	6	54%	13	--	13	6	14
4. 20 GeV/c beam	37%	7	10	27	16	4	50%	7	--	31	8	6	50%	7	--	31	3	10
5. B_Z = 15 kG in solenoid	27%	12%	17%	15%	25%	4%	42%	12%	--	20%	16%	10%	43%	12%	--	20%	8%	16%
6. B_Z = 50 kG in solenoid	57%	3	6	20	12	2	69%	3	--	22	2	3	70%	3	--	22	1	4
7. $\Delta P/P < 1/2\%$ in solenoid	27%	9	16	17	28	5	42%	9	--	21	18	10	43%	9	--	21	10	17
8. $\Delta P/P < 3\%$ in solenoid	60%	9	7	17	7	--	69%	9	--	21	--	--	69%	9	--	21	--	1
9. No solenoid measurement used	17%	9	18	17	34	5	30%	9	--	21	28	11	31%	9	--	21	20	19
10. r = 0.50 m in solenoid	29%	27	6	15	20	--	40%	27	--	17	9	6	43%	27	--	17	1	11
11. r = 1.00 m in solenoid	39%	3	15	17	22	4	52%	3	5	20	13	6	57%	3	1	22	5	13
12. ΔZ = 2 m in Gap 1	29%	9%	27%	13%	21%	2%	49%	9%	3%	20%	13%	6%	50%	9%	2%	21%	7%	12%
13. ΔZ = 3 m in Gap 1	23%	8	42	9	16	1	45%	9	9	18	15	4	47%	9	5	19	9	11
14. $\Delta\theta$ = 0 mrad, beam plug	49%	9%	10%	--	28%	5%	69%	9%	--	--	13%	9%	70%	9%	--	--	5%	16%
15. $\Delta\theta$ = 15 mrad beam plug	45%	9	11	5	26	5	64%	9	--	6	12	9	65%	9	--	6	5	15
16. $\Delta\theta$ = 50 mrad beam plug	21%	9	15	38	15	2	33%	9	--	46	8	5	34%	9	--	46	3	8
17. B_Y = 20 kG in magnet	31%	9%	13%	17%	25%	6%	43%	9%	--	21%	15%	12%	43%	9%	--	21%	8%	19%
18. $\pm\Delta X \cdot \pm\Delta Y = 1 \times 1/2$ m in magnet	36%	9	12	17	22	4	36%	9	12	17	22	4	36%	9	12	17	22	4
19. $\pm\Delta X \cdot \pm\Delta Y = 1\frac{1}{2} \times 1/2$ m in magnet	36%	9	12	17	19	7	36%	9	12	17	19	7	36%	9	12	17	19	7
20. $\pm\Delta X \cdot \pm\Delta Y = 1\frac{1}{2} \times 1$ m in magnet	53%	9	--	21	5	13	53%	9	--	21	4	13	53%	9	--	21	4	13
Ideal System With																		
21. B_Z = 50 kG, B_Y = 20 kG, $\Delta\theta$ = 5 mrad	67%	3%	4%	1%	18%	7%	80%	3%	--	1%	7%	10%	80%	3%	--	1%	3%	13%

1901B24

TABLE II

Acceptance for Solenoid System vs No Solenoid System

(Assume 25 kG. 3m×1.5m solenoid, 15 kg. 2m magnet, $\Delta\theta$=30 mrad, 5m×4m S.C.)

System Parameters	% Acceptance	Percentage Losses in Sol.	Gap 1	Plug	Mag.	Gap 2
16 GeV/c						
1st Gap = 1m.						
Small magnet $\Delta X \cdot \Delta Y = \pm 1 \times 1/2$						
1. $\Delta P/P < 1\%$ in solenoid	36%	9%	13%	17%	22%	4%
2. $\Delta P/P < 3\%$ in solenoid	60%	9	7	17	7	--
3. NO SOLENOID	17%	X	40	15	25	4
Large magnet $\Delta X \cdot \Delta Y = \pm 1\frac{1}{2} \times 1$						
4. $\Delta P/P < 1\%$	53%	9	--	21	4	13
5. $\Delta P/P < 3\%$	69%	9	--	21	--	1
6. NO SOLENOID	33%	X	10	21	20	16
1st Gap = 2m.						
Small magnet $\Delta X \cdot \Delta Y = \pm 1 \times 1/2$						
7. $\Delta P/P < 1\%$	29%	9	27	13	21	2
8. $\Delta P/P < 3\%$	53%	9	16	13	9	1
9. NO SOLENOID	16%	X	54	3	25	2
Large magnet $\Delta X \cdot \Delta Y = \pm 1\frac{1}{2} \times 1$						
10. $\Delta P/P < 1\%$	50%	9	2	21	7	12
11. $\Delta P/P < 3\%$	69%	9	1	21	--	1
12. NO SOLENOID	36%	X	18	5	25	16
8 GeV/c						
1st Gap = 1m.						
Small magnet $\pm 1 \times 1/2$						
13. $\Delta P/P < 1\%$	27%	25	24	3	20	1
14. $\Delta P/P < 3\%$	69%	25	3	3	--	--
15. NO SOLENOID	1/2%	X	87	1	12	--
Large magnet $\pm 1\frac{1}{2} \times 1$						
16. $\Delta P/P < 1\%$	45%	25	--	5	14	11
17. $\Delta P/P < 3\%$	69%	25	--	5	--	--
18. NO SOLENOID	5%	X	41	4	39	11
1st Gap = 2m.						
Small magnet $\pm 1 \times 1/2$						
19. $\Delta P/P < 1\%$	24%	25	40	--	10	--
20. $\Delta P/P < 3\%$	72%	25	2	--	--	--
21. NO SOLENOID	0%	X	95	--	5	--
Large magnet $\pm 1\frac{1}{2} \times 1$						
22. $\Delta P/P < 1\%$	44%	25	3	1	19	7
23. $\Delta P/P < 3\%$	73%	25	--	1	--	--
24. NO SOLENOID	4%	X	59	2	31	5

7. Ideal System

Line 21 in Table I suggests that if we could get a 50 kG solenoid and have very small beam plug (5 mrad), the acceptance figures would be 70% or better and there would be little need for a large magnet (in this final state).

8. Limiting Apertures

If we define the limiting aperture as the spectrometer component where substantial event loss ($\gtrsim$ 20%) takes place, then the conclusions are:

"Limiting aperture"	→	Conditions
a. solenoid		if $r \lesssim .50$ meters or if $p \lesssim 8$ GeV/c for beam
b. 1st gap		if ΔX, ΔY small and $P \leq 8$ GeV/c
		if ΔX, ΔY small and $\Delta Z \geq 2$ meters
c. plug		if ≥ 16 GeV/c and $\Delta\theta \geq 20$ mrads
d. magnet		if ΔX, ΔY small and $\Delta P/P \leq 1\%$

D. High Mass Acceptance

We now examine the solenoid-spectrometer acceptance efficiencies of 3π masses up to 3 - 4 GeV/c^2 at 8 and 16 GeV/c beam momentum. The previous comments referred to 3π masses as high as 1.5 GeV/c^2. This division in mass is somewhat artificial and is mainly the result of a different Monte Carlo procedure in the event simulation.[5]

The very dramatic effect of the solenoid is shown in Fig. 12. Even a large gap dipole magnet (3 m × 2 m) is helpless at high masses ($m(\pi\pi\pi) > 1.8$ GeV/c) without the solenoid as a vertex detector.

That is, the aperture burden shifts very sharply from the gap magnet at low masses to the solenoid at high masses.

Table III summarizes the acceptances for the small aperture (2 m × 1 m total $\Delta Y \cdot \Delta Y$) gap magnet. It is acceptable if coupled to the proposed solenoid. A minimum solenoid of 25 kG × 2 m diameter is recommended from this high mass study because a 1.5 m solenoid would have a very high loss rate at large masses.

At high masses about 40% of the events have a pion with $P_Z \lesssim 0$ (i.e., backward) and so is an automatic loss in our acceptance definition. This becomes the largest single main loss. Tables III and IV examine the solenoid losses more closely.

TABLE III

Abstracted Summary of Acceptances for Solenoid Magnet System vs $\pi\pi\pi$ Mass

System Parameters	% Acceptance	Percentage Losses in				
		Sol.	Gap 1	Plug	Mag.	Gap 2
1. 16 GeV: B_Z =25 kG, r=100 cm						
$\Delta P/P < 1\%$, $\Delta Z_1 = 2m$,						
$\Delta\theta = 0$ mrad, $B_Y = 15$ kG,						
$\pm\Delta X \cdot \Delta Y = 1 \cdot 1/2$m. Mag. Aperture						
Low Mass < 1.5 GeV/c	58%	0%	14%	X	26%	2%
Med. Mass 1.5 - 2.5	55%	19%	23%	X	4%	0%
High Mass > 2.5	21%	73%	5%	X	0%	0%
2. 8 GeV: B_Z = 25 kG, r = 100 cm						
$\Delta P/P < 1\%$, $\Delta Z_1 = 2m$,						
$\Delta\theta = 0$ mrad, $B_Y = 15$ kG,						
$\pm\Delta X \cdot \Delta Y = 1 \cdot 1/2$ m. Mag. Aperture						
Low Mass < 1.5	44%	2%	40%	X	13%	1%
Med. Mass 1.5 - 2.1	32%	43	25	X	0	0
High Mass > 2.1	12%	81	7	X	0	0
LARGER SOLENOID						
3. Sol_r = 125 cm, rest as in 1.						
16 GeV High Mass > 2.5	35%	57%	8%	X	0	0
8 GeV High Mass > 2.1	22%	65	12	X	0	0
LARGER MAGNET						
4. Mag $\pm\Delta X \cdot \Delta Y = 1\frac{1}{2} \cdot 1$ m, rest as in 1.						
16 GeV Low Mass < 1.5	87%	0%	0%	X	4%	10%
8 GeV Low Mass < 1.5	73%	2	4	X	12	9
$\Delta P/P$ LARGER						
5. $\Delta P/P < 3\%$ in solenoid, rest as in 1.						
16 GeV Low Mass	87%	0%	2%	X	10%	1%
Med. Mass	72%	19	7	X	1	0
8 GeV Low Mass	86%	2	8	X	3	0
Med. Mass	50%	43	7	X	0	0

TABLE IV

Solenoid Losses vs Z Axis Length

Target parameters 4 cm × 50 cm

Solenoid parameters 25 kG × 100 cm (radius)

Event Sample and $\pi\pi\pi$ masses	Total Loss at Z = (due to P_Z distributions)				
	.5m	1.0m	1.75m	2.25m	3.0m EXIT
16 GeV/c Med. Mass (1.5-2.5)	1%	1%	2%	8%	19%
16 GeV/c High Mass (> 2.5)	38%	48%	64%	69%	73%
8 GeV/c Med. Mass (1.5-2.1)	8%	9%	20%	30%	43%
8 GeV/c High Mass (> 2.1)	43%	58%	74%	78%	81%

E. Conclusions

1. The solenoid-magnet system studied here has an event acceptance range 17% to 80% for the $A \rightarrow \pi\pi\pi$ mass region.

2. We find that the solenoid is absolutely essential for acceptances of masses above 1.8 GeV/c^2.

3. A minimum solenoid of 25 kG × 2 m diameter is recommended.

4. The small aperture (2 m × 1 m total $\Delta X \cdot \Delta Y$) gap magnet is acceptable if coupled to the proposed solenoid.

5. Without a solenoid, there are serious dead regions in $\cos \theta = \pm 1$ for the decays. The solenoid helps fill these in.

6. A good solenoid ($\geq$ .75 m and B_Z > 25 kG) does reduce the large aperture need of the big magnet. The solenoid increases the overall system acceptance.

7. A large solenoid field is a more important parameter than the solenoid aperture. The field adds to acceptance and resolution, the latter mostly to acceptance.

8. The beam "plug" losses are appreciable above 16 GeV/c if the plug is more than ± 20 mrad. This is a problem independent of the solenoid and magnet.

IV. TRACK RESOLUTION INSIDE THE SOLENOID

To help evaluate the potential usefulness of the solenoid further we now address ourselves to some other specific questions. They are:

What momentum resolution can we expect in P_T, P_L, and P for tracks measured inside the solenoid?

How does the resolution vary with P_T, P_L, and the solenoid field B and length Z?

What would a realistic B_Z and B_r field map look like for the solenoid?

How does this compare with the "box field" approximation in the fitting for P_T and P_L?

What does the azimuthal uncertainty $\Delta\phi$ do to the mass resolution?

Additional questions should also be considered. The effect of the least squares fitting to the vertex, the solenoid fringe field integration for fast tracks and the multiple scattering in the target and chambers are some examples, but they are not examined in this report.

A. Momentum Resolution

1. Procedure

The following procedure was used to find the momentum resolution of typical trajectories.

A particle with fixed P_T and P_L was traced through a fixed and uniform B_Z magnetic field of a solenoid. The X and Y intercepts of this trajectory were found at Z values corresponding to spark chamber planes. Next the exact X, Y, and Z intercept points are displaced from their true value. This displacement is given a random but Gaussian distribution. The width of the Gaussian is called the "spark accuracy."

The new set of points are then fed into a least squares circle fitting routine[6] and the fitted radius R then gives a "measured" P_T.

Transverse momentum resolution is defined as

$$\Delta P_T = P_T(\text{original}) - P_T(\text{measured}) \quad . \tag{9}$$

The longitudinal momentum P_L is found from 2 consecutive planes via

$$\frac{P_L}{P_T} = \frac{z_0}{A} = \frac{z_0}{R\Delta\phi} \tag{10}$$

z_0 = spacing between planes along Z axis, $\Delta\phi$ = angle subtended by arc in XY plane between the same 2 planes. The "measured" P_L is then taken as the average

$$P_L = \frac{\sum_{i=1}^{N-1} P_L^i}{N-1} \tag{11}$$

N = the number of planes (N-1 arcs). The overall momentum is $P = \sqrt{P_T^2 + P_L^2}$

$$\Delta P = P \text{ (original)} - P \text{ (measured)} \quad . \tag{12}$$

2. P Resolution Comments

The orthogonal variables P_T and P_L are measured directly and from this one can calculate the dip angle λ and the total momentum P.

P_T is measured by the radius of the circle in the XY plane. Its accuracy thus depends on the value of the spark uncertainty dx and dy, the field map uncertainty dB and the multiple scattering. It does not depend on the dz uncertainty of the chambers (insofar as B and dB do not).

P_L is determined from the measured P_T value and from the spark chamber separation ΔZ. Thus it has errors from two sources, from dP_T and from dz.

3. P_T Resolution

For the moment let us assume that the solenoid B field is well known and that the only error in the determination of P_T comes from R. The following algebra derives the resolution dependence

$$P_T = \frac{1}{a_0} BR \qquad a_0 = 33.36 \tag{13}$$

For the arc fitting procedure in the XY plane

$$R = \frac{C^2}{8S} + \frac{S}{2} \tag{14}$$

where C = the chord length, S = the sagitta of the chord

$$C = r = \sqrt{X^2 + Y^2}$$

$$= 2a_0 \frac{P_T}{B} \sin\left(\frac{BZ}{2a_0 P_L}\right) \tag{15}$$

For small arcs in the XY plane (i.e., $P_L > P_T$) we keep only the first term in (14) and expand $\sin \alpha \approx \alpha$ in (15) to obtain

$$P_T = \frac{8a_0}{B}\left[\frac{P_L}{Z}\right]^2 S \tag{16}$$

and thus the error dP_T varies directly as the sagitta uncertainty dS. The dS uncertainty should be approximately equal to the spark uncertainty in the XY plane.

The dP_T dependence on B, P_L, Z and dS, given by Eq. (16), has also been verified with a Monte Carlo simulation. The results are listed in Table V. The listed $\pm\sigma$ for the momentum resolution are found by visual fits to the ΔP histograms and so are only approximately exact.

The first line in Table V illustrates a typical value of ± 3 MeV in dP_T when P_T = 300 MeV, P_L = 1500 MeV, in a solenoid with length ΔZ = 2.5 meters, field B = 25 kilogauss and a spark jitter of $\pm$ 1 mm in the X and Y directions. That is dP_T/P_T is found to be 1% for these representative parameters.

The other lines in Table V show how dP_T then varies as the parameters are changed.

It turns out that the momentum resolution is not very sensitive to the number of planes. Six planes and three planes over the same solenoid length give essentially the same resolution. Lines 9 and 10 in Table V show that by doubling the number of planes (3 planes in line 9 and 6 in 10) we improve dP_T by about 20%. It may go as $\sqrt{N}$, where N is the number of planes. Because of this weak dependence, only the 6 plane data (except for line 9) is shown in Table V.

In a real experiment one gets several sparks per spark chamber and there then is a pattern recognition problem in the XY plane. Any 3 sparks can define an arc and by having some redundancy in the sparks (say 4 planes) the pattern recognition should be easier. This problem is examined in more detail in Chapter V.

TABLE V

SOLENOID ΔP RESOLUTION

	INPUT						OUTPUT			
	Particle Momentum		B Field Length		S.C. Resolution dx=dy	dz	Momentum Resolution ΔP_T	ΔP_L	ΔP	$\Delta P/P$
	P_T (GeV)	P_L (GeV)	ΔZ (m)	B (kG)	$\pm\sigma$ (mm)	$\pm\sigma$ (mm)	$\pm\sigma$ (MeV)	$\pm\sigma$ (MeV)	$\pm\sigma$ (MeV)	%
1	.3	1.5	2.5	25	1	0	3	NM	19	1.5
2	.3	1.5	2.5	50	1	0	1.6	10	10	.6
3	.3	1.5	2.5	25	.5	0	1.6	10	10	.6
4	.3	1.5	2.5	25	0	2	0	1.6	1.6	.1
5	.3	1.5	2.5	25	0	6	0	5	5	.3
6	.3	1.5	2.5	25	1	6	3	NM	20	1.3
7	.3	1.5	5.0	25	1	0	<1	NM	5	.3
8	.3	1.5	1.25	25	1	0	13	NM	76	5
9 *	.3	1.5	1.0	25	1	0	26	NM	150	10
10	.3	1.5	1.0	25	1	0	20	NM	120	8
11	.3	1.0	2.5	25	1	0	1.5	NM	6	6
12	.3	0.5	2.5	25	1	0	<1	NM	.7	.1
13	1.5	1.50	2.5	25	1	0	4	NM	38	2.5
14	.3	1.50	2.5	25	0	6	0	3	3	2.5

(NM for not measured directly)
*3 chambers along Z axis

4. P_L Resolution

The longitudinal momentum is easily found via

$$\frac{P_L}{P_T} = \frac{Z}{A}$$

Z is Z axis length in solenoid, A is the arc length in XY plane

$$P_L = \frac{P_T}{A} \cdot Z$$

Thus if there was zero error in P_T, dP_L would depend directly on dZ. On the other hand, if dZ = 0, dP_L varies with dP_T

$$\frac{dP_L}{dP_T} \approx \frac{Z}{A} = \frac{P_L}{P_T} \tag{17}$$

Table V illustrates both dependencies. Unless dZ is very large in comparison to dS ($\gtrsim$ 6 times) or unless P_L is small, the dominant contribution to dP_L comes from dP_T. The table bears this out.

In addition to dP_T and dP_L the table shows what the corresponding total dP is and also expresses this as a percent error in P.

The overall conclusion is that the results look extremely good for $\Delta P/P$ and a 3 m × 25 kG type of solenoid.

Another interesting feature is that if one should desire to use the solenoid for high energy particles, say 10 GeV, simply scale the length accordingly (3 × 10 = 30 meters) and one can in principle maintain the same $\Delta P/P$ accuracy. This follows from Eq. (16)

$$\frac{\Delta P}{P} \propto \left(\frac{P_L}{\Delta Z}\right)^2 \quad . \tag{18}$$

B. Solenoid Field Map

To get some idea on how a more realistic solenoid field map would look, one can construct a typical coil geometry and integrate the B_z and B_r values throughout the solenoid volume. Figure 16 shows such a coil geometry.[7] Three 25 cm wide gaps are shown for the spark chambers. The corresponding B_z map inside the .8 m × 3.0 m plane of r-z and the B_r map are shown in Fig. 16.

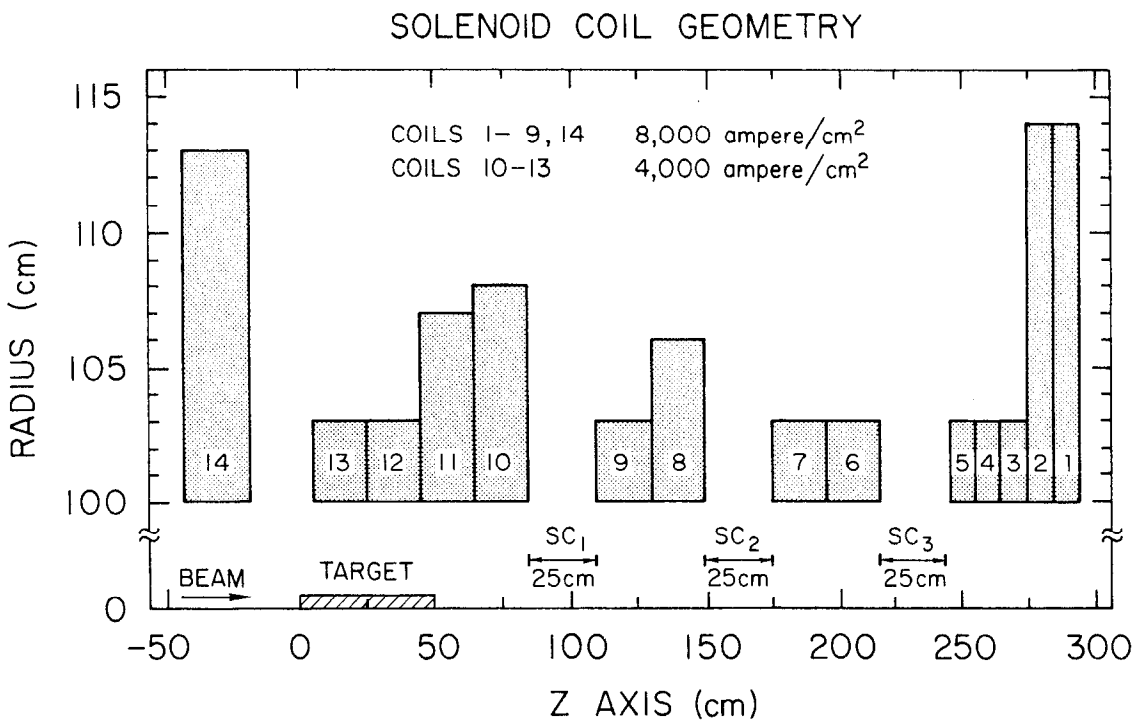

B_Z FIELD MAP (IN kG) INSIDE SOLENOID									
Z axis (cm) / Radius (cm)	0	20	60	100	140	180	220	260	300
80	25.70	23.58	25.79	22.96	27.58	24.52	22.80	31.67	23.85
60	26.17	24.92	25.02	24.63	25.82	24.78	24.71	27.98	22.52
40	25.54	25.17	24.94	24.96	25.37	24.97	25.16	26.02	21.36
30	25.26	25.14	24.95	25.01	25.28	25.02	25.22	25.45	20.99
20	25.05	25.11	24.96	25.03	25.24	25.06	25.23	25.08	20.74
10	24.93	25.08	24.97	25.04	25.21	25.08	25.22	24.87	20.60
0	24.89	25.07	24.97	25.05	25.20	25.08	25.22	24.80	20.55

B_r FIELD MAP (IN kG)									
Radius (cm) /				SC_1		SC_2		SC_3	
80	-3.40	-.87	.06	.99	-1.11	.52	.42	2.85	-12.30
60	-.74	-.51	-.06	.39	-.21	-.11	.59	-.12	-6.54
40	.09	-.16	-.04	.16	-.04	-.07	.28	-.65	-3.61
30	.19	-.06	-.03	.10	-.02	-.04	.17	-.59	-2.56
20	.18	-.02	-.02	.06	-.01	-.02	.09	-.44	-1.64
10	.10	.0	-.01	.03	.0	-.10	.04	-.23	-.81
0	.0	.0	.0	.0	.0	.0	.0	.0	.0

1901C5

FIG. 16--A typical solenoid coil geometry for a superconducting 25 kG field and field map B_Z vs Z and r inside solenoid; field map B_r vs Z and r inside solenoid.

The B_z = 25 kG is within 1% for the first 10 cm around the solenoid axis. Near r = 80 cm the B_z nonuniformity is of the order of 10%. This field map assumes no iron shielding — and therefore is not reliable in a fringe field study.

C. Real Field Versus Box Field

Given the usual Monte Carlo events generated at the target, it is very easy to integrate the pions through the solenoid by two different procedures and then compare the results.

Procedure A is the ideal box field approximation we have been using.

Procedure B is the more "exact" or realistic approximation. It uses a field map determined from the above first guess at the real coil configurations and then integrates each track.

A typical distribution showing the difference in P_T for the two procedures and for slow pions is illustrated in Fig. 17. It has a reasonable fit to a gaussian and gives $\Gamma = 0.85$ MeV. This fit is summarized in line 1 of Table VI.B. By "slow" pions here one means $P < 1$ GeV/c and the integration is taken through $\Delta Z = 2.5$ m to the 3rd spark chamber. The other lines in this table correspond to similar fits for different momentum pions. The very interesting point is that even for slow pions, which are swept out to the edge of the solenoid and whose momenta must be measured by the solenoid, a box field approximation to the field reproduces the P_T to within 1 MeV, $\Delta P_z \approx .25$ MeV, and ΔX at the 3rd spark chamber to within 1.2 mm.

All differences are reduced if we look at the 2nd chamber values (Table VI.A).

The P_T rotation angle uncertainty $d\phi \approx 20$ mrad for slow pions corresponds to a maximum invariant mass width of about ±2 MeV and thus is not disastrous.

In practice one can certainly use a 2, 3, or 5 connected "box" integrations through the solenoid and thus reduce the above differences.

The fast tracks, which do not usually get past r = 20 cm from the solenoid axis have a very uniform field and so have excellent results for the box approximation, e.g., $\Delta x \approx \pm .03$ mm for the spatial deviation. This is certainly within any possible resolution.

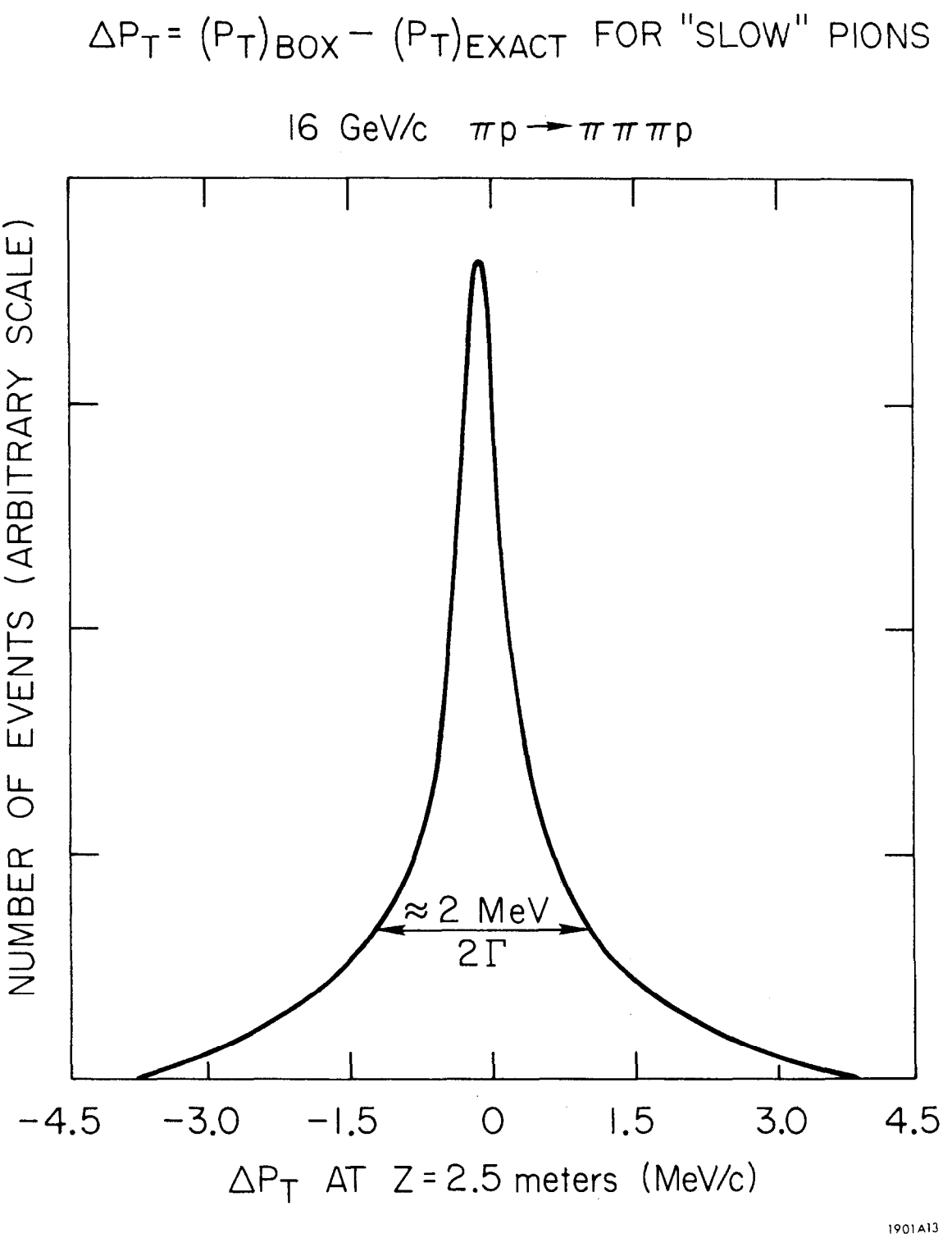

FIG. 17--Solenoid P_T resolution for slow pions in 16 GeV/c $\pi p \rightarrow \pi\pi\pi p$.

TABLE VI

RESOLUTION HALFWIDTHS DUE TO SOLENOID
BOX FIELD APPROXIMATION

(Γ from ($X_{BOX} - X_{EXACT}$))

A. At Z = 1.5 m (2nd Spark Chamber)						
Width Γ / Pion Mom.	ΔP_z (MeV)	$\Delta P_\perp$ (MeV)	$\Delta\varphi$ (mrad)	$\Delta\theta$ (mrad)	ΔX (mm)	Δr (mm)
A. P>1 GeV	0.10	0.33	5.21	0.63	0.29	0.68
B. 1-2 GeV	0.05	0.30	1.96	0.22	0.10	0.41
C. 2-4 GeV	0.02	0.21	0.95	0.07	0.03	0.28
D. P>4 GeV	0.01	0.11	0.43	0.02	0.01	0.15
B. At Z = 2.5 m (3rd Spark Chamber)						
A. Slow Pions	0.27	0.85	18.80	1.68	1.16	1.76
B. Med. Pions	0.16	0.75	7.46	0.56	0.41	1.00
C. Med. Pions	0.05	0.36	3.30	0.13	0.13	0.51
D. Fast Pions	0.01	0.20	1.30	0.03	0.03	0.27

Figure 18 sketches the $\Delta\phi$, θ and $r = X^2 + Y^2$ variable distributions — for which Table VI.B lists the reconstruction "errors."

Note that event the fast tracks are rotated through a ϕ angle of 5^o - 25^o. (Bottom-left sketch in Fig. 18.)

Conclusions

1. It appears that our simplifying approximation of a box field (B_z = 25 kG, $B_r = 0$) inside the solenoid is a very good approximation to a real coil field and a step wise integration through it. It is best for the fast tracks which only see the very uniform field near the center axis. This means that lengthy "tracking" inside the solenoid is unnecessary and should minimize the computing needs.

2. The following few figures illustrate and summarize how the B_z = 25 kG, $B_r = 0$, one-step integration compares with a 4th order Runge-Kutta integration through the real field map. The track path length used is $z \approx 2.5$ meters (i.e., from target to third spark chamber).

	Halfwidths for $(X_{BOX} - X_{EXACT}) =$				
	ΔP_z	ΔP	$\Delta\phi$	$\Delta\theta$	ΔX
	MeV	MeV	mrad	mrad	mm
A. Fast tracks (P > 4 GeV)	.01	.2	1.3	.03	.03
B. Medium tracks (1 - 4 GeV)	.11	.6	6.0	.4	.3
C. Slow tracks (< 1 GeV)	.27	.9	19.0	1.7	1.2

D. Some $d\phi$ Comments

The B_Z (axial B field) of a solenoid, which rotates the P_T (transverse momentum) of the particles, can introduce substantial $\Delta\phi$ errors in the reconstruction of P_X and P_Y at the vertex

$$P_X = P_T \cos\phi$$

$$P_Y = P_T \sin\phi$$

The error $\pm d\phi$ may be as large as 5 - 10 milliradians at the vertex. For example, an error of $\Delta B/B \approx 1\%$ will produce an error in $d\phi$ of about ± 7 milliradians over 75 kG-m.

It turns out, however, that if P_T and P_L are kept invariant in the reconstruction (which is what a pure B_Z field does), the mass resolution is not very sensitive to $\pm d\phi$.

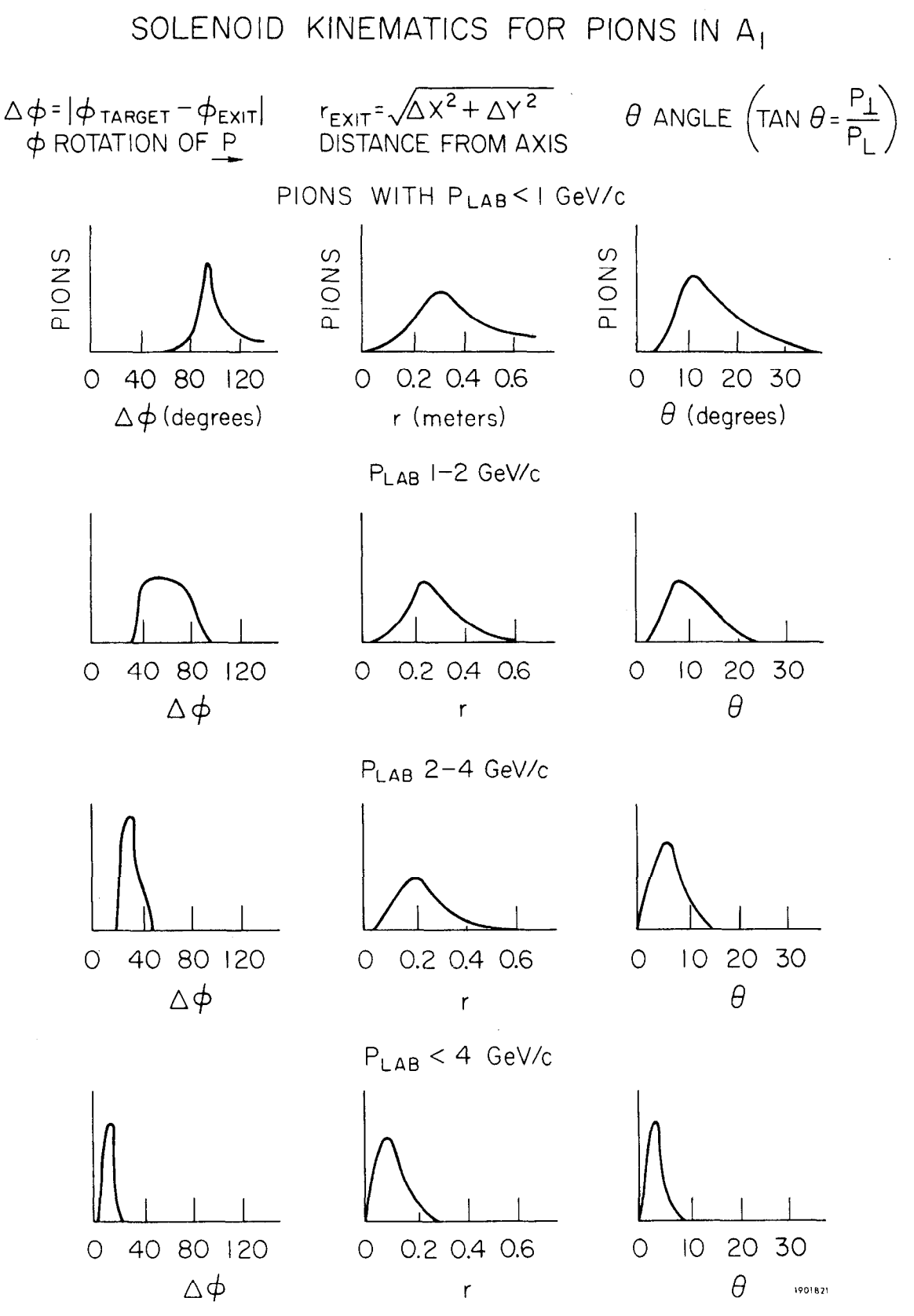

FIG. 18--Particle kinematics inside solenoid as a function of their lab momentum.

A $\pm d\phi$ = 7 mrad implies $\pm\Delta$ mass $\lesssim$ .7 MeV/c^2 for the $\rho \rightarrow \pi\pi$ ($\approx$ 750 MeV/c^2).

Table VII summarizes these results.

In the two particle case, a little algebra leads to

$$\Delta M_{12} \approx -\left(\frac{P_{1T}P_{2T}}{M_{12}}\right) \sin(\phi_1-\phi_2)\,(\Delta\phi_1-\Delta\phi_2) \qquad (19)$$

The labels 1 and 2 refer to particles 1 and 2 respectively. This ΔM expression is consistent with the Monte Carlo determination of Table VII. The fact that P_T has an upper bound of about .5 GeV/c reflects in a small ΔM.

Thus even though the $\Delta\phi$ variations may be extremely large by comparison with conventional spectrometer, the solenoid would still have good mass resolution. A word of caution, however, since this example idealizes the situation. The fast track in fact will probably have to be integrated through the exit fringe field to determine P_T.

TABLE VII

$\pm \Delta\phi$ Jitter at Vertex vs ΔP_X and Δmass for Three Pions in 16 GeV/c

$\pi p \rightarrow \pi_1 \pi_2 \pi_3 p$ (i.e., P_Z and $P_\perp$ of Particles Remain Invariant)

INPUT	OUTPUT			
$\pm \Delta\phi$ Jitter (mrad)	$\pm \Delta P_X$ (MeV)	$\pm \Sigma\Delta P_X$ (MeV)	$\pm \Delta M(\pi_1 \pi_2)$ (MeV)	$\pm \Delta M(\pi_1 \pi_2 \pi_3)$ (MeV)
0.0	0.0004	0.0004	0.002	0.0003
0.2	0.02	0.07	0.03	0.03
1	0.14	0.31	0.1	0.06
3	0.4	0.9	0.3	0.2
5	0.7	1.7	0.5	0.3
20	3.5	11	2.2	1.5
100	18	42	10	6

V. PATTERN RECOGNITION

A very important consideration for any high statistics counter experiment is one of computing needs. Related to this is the question of recognizing track patterns among the many sparks recorded in the spark chambers. The questions are, how well can one find the sparks for a track and how long does this take?

The following discussion shows that the very simple procedure of looking for proportional (or equal) chord lengths in the XY plane of the solenoid gives satisfactory results and with a minimum of computing time.

Table VIII summarizes the results of this algorithm in regards to the track recognition efficiency. The computing time is 30 microseconds on the 360-91 to calculate a 3-spark search parameter. Thus

(a) if 1 event $\equiv (4 \times 4 \times 4)$ sparks in 3 planes => 2 msec/event,

(b) if 1 event $\equiv (6 \times 6 \times 6)$ sparks in 3 planes => 6-1/2 msec/event.

This timing comes from a Fortran coding of the calculation.

Two other conclusions are:

(1) It is better to have evenly spaced chambers along the solenoid axis. This simplifies the algorithm and makes it a better approximation,

(2) The track recognition signal is strongly dependent on the ΔX and ΔY jitter of the sparks in the chambers. This is demonstrated in Table VIII.

No check has been made on how variations in B_Z or $B_r \neq 0$ affect the results.

The number of sparks combinations can be reduced by various criteria. A simple suggestion is presented. It reduces the number, improves the signal to noise but does reduce the signal some.

A. The Algorithm

A perfectly axial B_Z field rotates the P_T momentum vector of a particle and leaves the magnitudes of P_T and P_Z invariant.

Thus for a particle inside the solenoid, P_T/P_Z is invariant. Consider this ratio when the particle passes from one spark chamber plane to the next (i.e., plane 1 → 2)

$$\frac{P_T}{P_Z} = \frac{mV_T}{mV_Z} = \frac{S_{12}/\Delta t}{Z_{12}/\Delta t} = \frac{S_{12}}{Z_{12}} \tag{20}$$

TABLE VIII

Solenoid Track Recognition Efficiency

($\pi^- p \rightarrow \pi_1^- \pi_2^+ \pi_3^- p$ 4 Sparks/Plane and 3 Planes/Event, using all 12 sparks per event)

	INPUT	OUTPUT						
	Beam, Solenoid, Chamber and Spark Conditions	Γ_R Signal	R = .75 - 1.25		R = .90 - 1.10		R = .95 - 1.05	
			%Sig.	NOISE / RL TRKS	%Sig.	NOISE / RL TRKS	%Sig.	NOISE / RL TRKS
1.	16 GeV/c, 25 kG, $Z_{12} = Z_{23} = 1$ m $\Delta X = \Delta Y = \Delta Z = 0$	.001	100	1.8	100	.7	100	.4
2.	16 GeV/c, 25 kG, $Z_{12} = Z_{23} = 1$ m $\Delta X = \Delta Y = 0$ $\Delta Z = \pm 2$ mm	.01	100	1.8	100	.7	100	.4
3.	16 GeV/c, 25 kG, $Z_{12} = Z_{23} = 1$ m $\Delta X = \Delta Y = \pm 1$ mm $\Delta Z = \pm 2$ mm	.025	96	1.8	83	.9	66	.6
4.	16 GeV/c, 25 kG $Z_{12} = Z_{23} = 1$ m $\Delta X = \Delta Y = \pm 2$ mm $\Delta Z = \pm 4$ mm	.045	88	2.0	66	1.1	48	.7
5.	16 GeV/c, 25 kG, $Z_{12} = 1.25$, $Z_{23} = .75$ mm $\Delta X = \Delta Y = \pm 1$ mm $\Delta Z = \pm 2$ mm	.06	71	.7	56	.5	37	.4
6.	16 GeV/c, 50 kG $Z_{12} = Z_{23} = 1$ m $\Delta X = \Delta Y = \pm 1$ mm $\Delta Z = \pm 2$ mm	.025	95	1.8	82	.9	64	.6
7.	8 GeV/c, 25 kG $Z_{12} = Z_{23} = 1$ m $\Delta X = \Delta Y = \pm 1$ mm $\Delta Z = \pm 2$ mm	.018	99	1.7	94	.7	81	.5
8.	8 GeV/c, 50 kG $Z_{12} = Z_{23} = 1$ m $\Delta X = \Delta Y = \pm 1$ mm $\Delta Z = \pm 2$ mm	.020	98	1.9	91	.9	78	.5
9.	$r_1 = X^2 + Y^2 > 5$ cm cut 16 GeV/c, 25 kG $Z_{12} = Z_{23} = 1$ m $\Delta X = \Delta Y = \pm 1$ mm $\Delta Z = \pm 2$ mm	.020	69	1.7	66	.7	56	.4

S_{12} is the arc length in plane XY, Z_{12} is the plane separation along the Z axis. Similarly for planes 2 → 3

$$\frac{P_T}{P_Z} = \frac{S_{12}}{Z_{12}} = \frac{S_{23}}{Z_{23}}$$

let

$$R = \frac{S_{12}/Z_{12}}{S_{23}/Z_{23}} \tag{21}$$

then $R = 1$ if we are joining sparks that belong to the same track, $R \neq 1$ if we are joining sparks that belong to different tracks, ($R \approx 1$ as some background), $S = R\,\Delta\phi$ in the XY plane, and if $\Delta\phi$ is small $S_{12} \approx A_{12}$, where A_{12} is the straight line segment from spark 1 → 2 in the XY plane.

$$R = \frac{A_{12}}{A_{23}} \frac{Z_{23}}{Z_{12}}$$

and if we label this variable (and square it to simplify the computing)

R_{ijk} i refers to the spark number in plane 1
j refers to the spark number in plane 2
k refers to the spark number in plane 3

$$R_{ijk} \approx \left(\frac{A_{12}^{ij}}{A_{23}^{jk}} \frac{Z_{23}^{jk}}{Z_{12}^{ij}} \right)^2 \tag{22}$$

The above defined variable R_{ijk} is called the 3-spark search parameter.

If the 3 planes are equally spaced, $(S_{12}/S_{23}) = (A_{12}/A_{23}) = 1$ exactly and we are not bothered by the $S_{12} = kA_{12}$ approximation.

That is, for evenly spaced solenoid chambers, our algorithm is simply the search for equidistant points in the XY plane.

B. Procedure and Results

The Monte Carlo simulation study used the following procedure.

(1) As described earlier in this report, a four-body event is generated in the target and the particles are traced through the solenoid. The spark chamber intercepts are then defined as "sparks."

(2) These sparks can then be displaced from their true position in X, Y, and Z by a gaussian error function.

(3) The four sparks from each solenoid chamber are then collected and all possible combinations of the R_{ijk} parameter are calculated (64 total for 4 sparks in each of 3 planes).

(4) Remembering which sparks really belonged to a track, one can then examine the resolution of the algorithm.

(5) No acceptance checks or measurement checks were made on the sparks or tracks in this chapter.

XY Plane Distribution of Sparks

The ease of recognizing tracks will depend strongly on the spatial distribution of the sparks in the three chambers.

In Fig. 19 one sees that a great many sparks occur within ±15 cm of the beam line. Many of these are due to the very fast pions (up to P_Z = 15 GeV/c) which will not be measured in the solenoid anyway.

Many of the large $r = \sqrt{X^2 + Y^2}$ points are due to the slow protons, which usually rotate more than π in the 2 meter ΔZ.

To remove some of the very fast tracks, one can simply check the r value of the spark and disregard it if it lies within some small circle (e.g., 5 - 10 cm from the center line). This reduces the number of combinations (i.e., computing time) and emphasizes the search for the slower tracks, which one is measuring in the solenoid.

If one wishes, a second pass search can then be made on the remaining and unassigned sparks.

Algorithm Results

We next look at the distributions of the R_{ijk} search parameter for a large number of events and sparks. Figure 20 shows how the parameter values distribute themselves when for each "real track" R_{ijk} one also plots fifteen "nontrack" R_{ijk}. In this figure the sparks are given a reasonable jitter of ±1 mm in X and in Y and ±2 mm in Z (gaussian σ values). If there was no such experimental jitter, one would see a very sharp delta function at R=1.

The background (i.e., 3-spark combinations for false tracks) peaks at low values of R and is reasonably flat and smooth under the "real track" signal

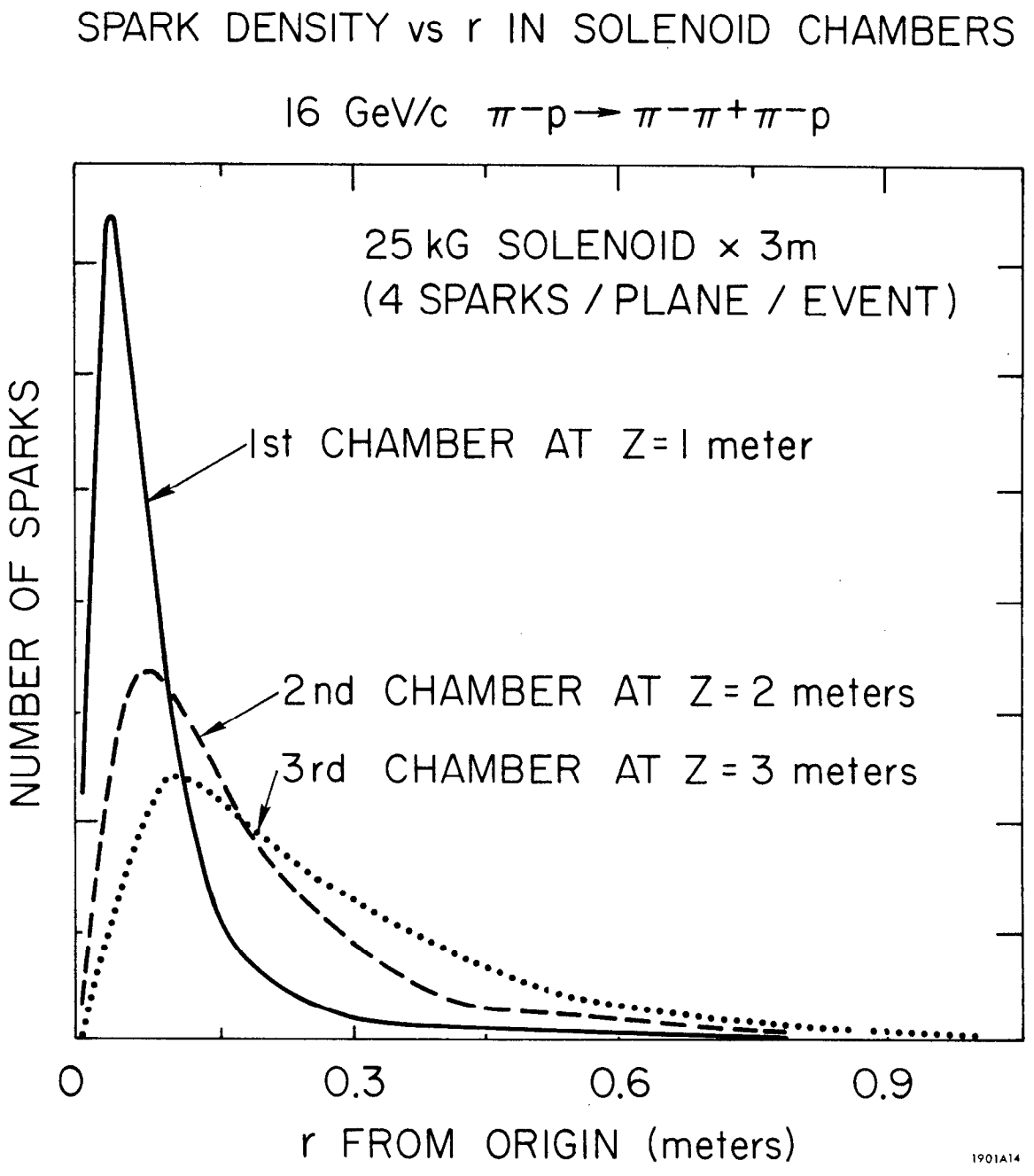

FIG. 19--Typical spark distributions (in radius r) at the 1st, 2nd, and 3rd spark chambers.

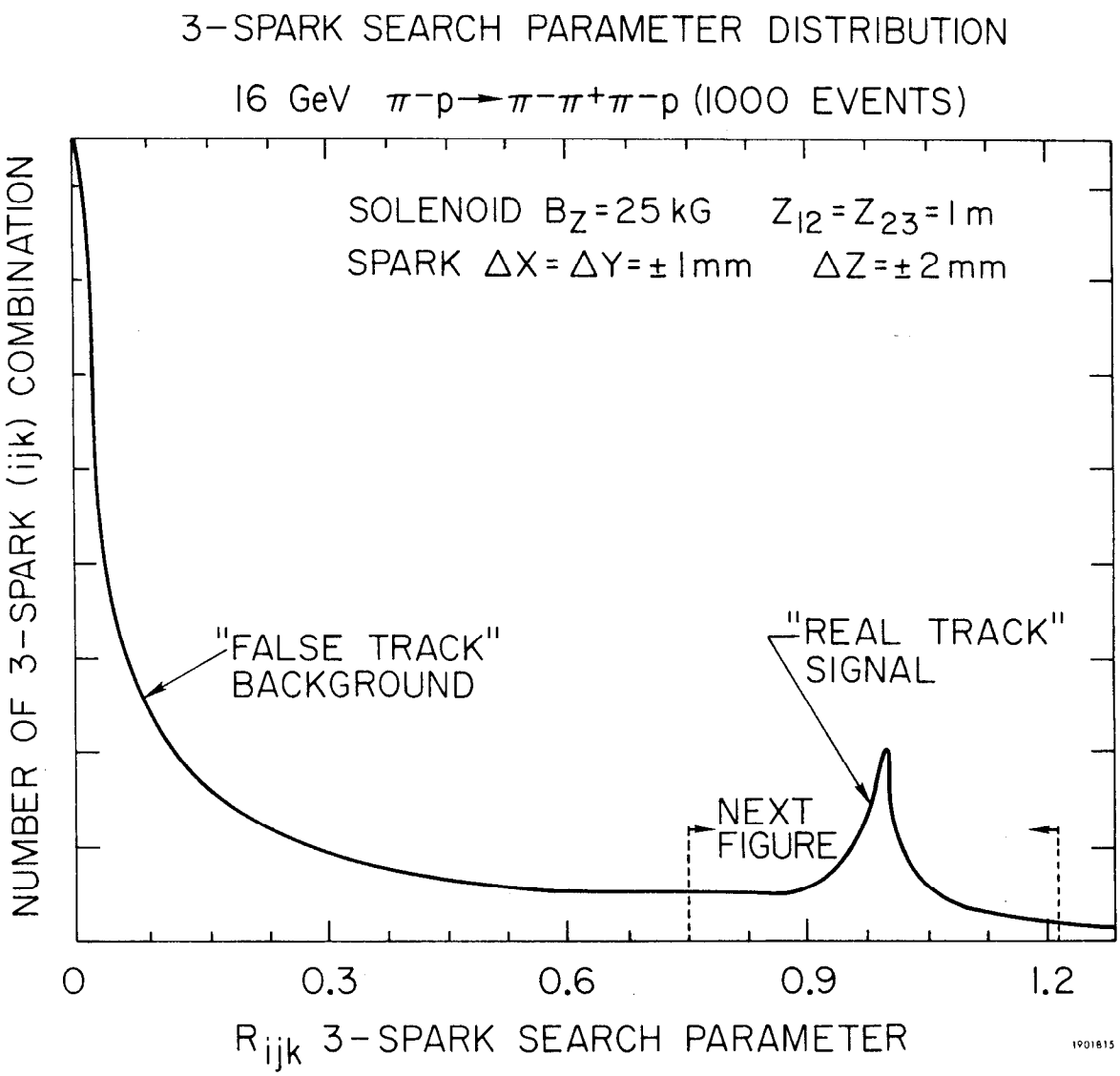

FIG. 20--Typical 3-spark search parameter distribution.

at $R \approx 1$. Thus one can quickly disregard all R_{ijk} values, i.e., all spark combinations, that are not near this signal.

Table VIII summarizes the percent of the signal as well as the noise to real track ratio for three different cuts on the R number. The wider this cut, the more signal one gets but the higher the background ratio. In Table VIII, the column labeled NOISE/RL TRKS is defined as

$$\frac{\text{NOISE}}{\text{RL TRKS}} = \frac{\text{(total number of combinations) - (real track combinations)}}{\text{(real track combinations)}}$$

The table also shows how these values depend on different experimental conditions. One observes that

(1) $\Delta Z = \pm 2$ mm jitter affects the very narrow R signal very slightly (case 2).

(2) The Γ_R appears to vary directly with the ΔX, ΔY errors in the sparks (case 3 and 4).

(3) The uneven chamber spacing (case 5) results in a drastic reduction of the signal. This is primarily due to the slow proton which now really needs a mod(2π) extension of the algorithm.

Because the proton tracks have such a low P_Z, their sparks are well separated in the XY plane and so R_{ijk} for the proton has a much better signal than for the pions.

(4) A 50 kG solenoid does not seem to affect the signal very much (case 6).

(5) A reduction of beam energy improves the signal somewhat. The tracks are slower in P_Z and so trace out a larger arc in the X-Y plane, which then is easier to find.

Figures 21a and 21b examine the R_{ijk} distribution near the signal in more detail. Figure 21a is a blow up of the $R = 0.75$ to 1.25 region from Fig. 20. It also shows what the real track signal looks like in the region of $R \approx 1$.

Figure 21b shows what the R distribution looks like when we reject all sparks in the first chamber within 5 cm of the center line. (See Fig. 19.) The background is reduced by about 50%, but the signal by only about 25%. Again, let us emphasize that this 25% is mainly from the very fast tracks which one will measure in the large magnet anyway. Figures 21a and 21b have the same event sample and the same axis' scales and so the signal sizes are directly comparable.

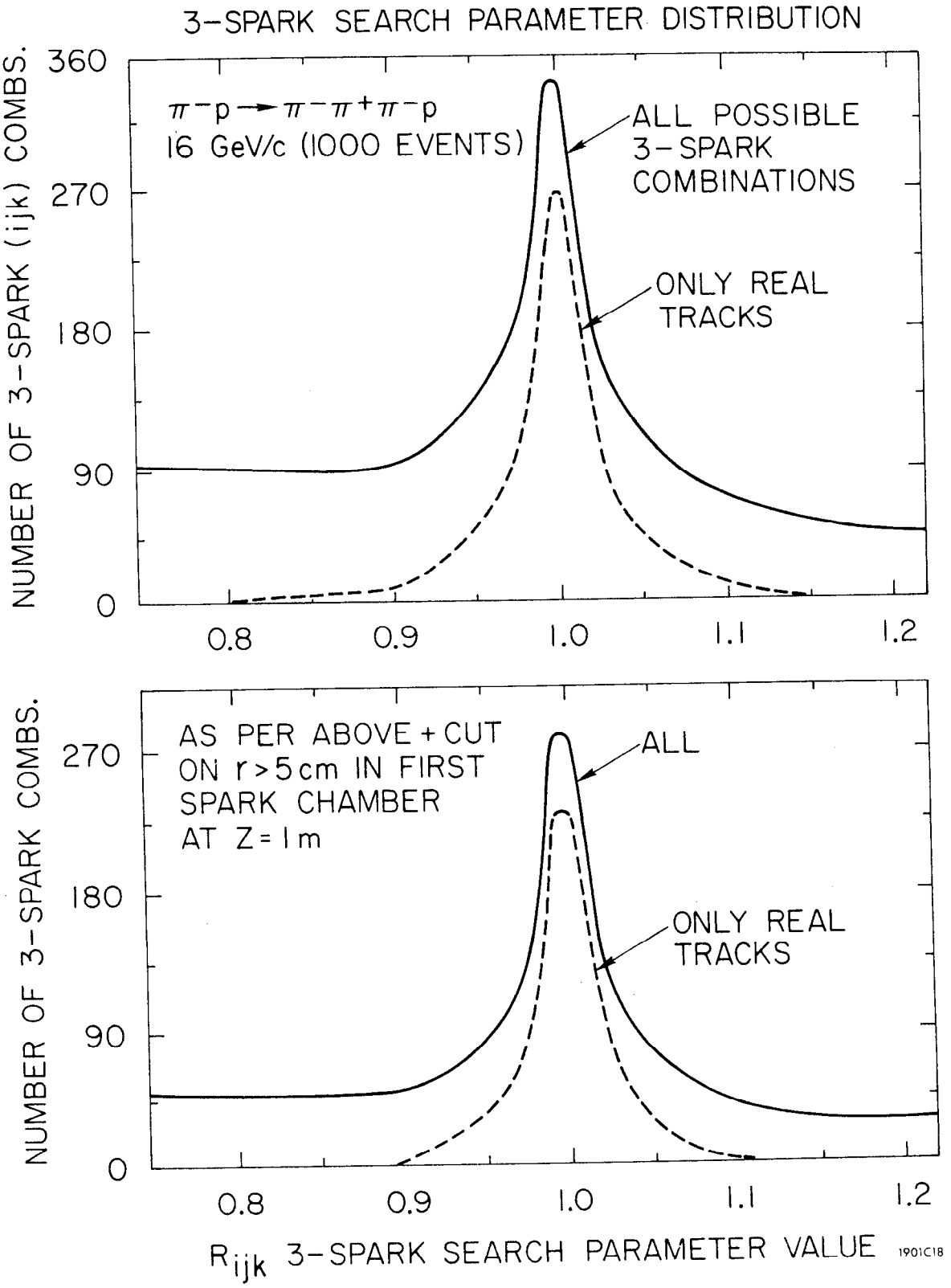

FIG. 21--3-spark search parameter distribution in the region of the signal.

Table VIII, case 9, shows the signal and noise/signal values with the $r_1 > 5$ cm cut on the sparks.

It is anticipated that after one has selected the spark combination with R in some region centered at 1, the background should be separable from the real tracks by doing a least squares fit in space and using a common vertex constraint. This has not been studied here.

REFERENCES

1. Multiparticle spectrometer references
   a. NAL 1969 Summer Study, Volume 3, Spectrometer Systems, pp. 165-335.
   b. NAL 1970 Summer Study "Vertex detectors employing magnetic fields along the beam axis," D. I. Meyer, p. 161.
   c. CERN Omega Project, NP Division, Internal Report 68-11 (1968).
   d. 1970 Philadelphia Conference, Experimental Meson Spectroscopy, ed. Baltay and Rosenfeld (Columbia University Press, New York, 1970). Band et al., "The CERN-IHEP boson spectrometer," p. 557; Ficenec et al., "Multiparticle spectrometer system for the 10 - 30 GeV/c region," p. 581; Leith and Luste, "SLAC large wire spark chamber spectrometer," p. 593; Lindenbaum, "Multiparticle magnetic spectrometer systems with electronic digitized detectors and on-line computer," p. 609.
2. SLAC Group B Spectrometer Memos, G. Luste
   a. "A_1-A_2 enhancement efficiencies for the proposed large magnet-spark chamber facility at SLAC" with L. Madansky, No. 36 (October 1969).
   b. "Solenoid-spark chamber system," No. 43-I (April 1970).
   c. "Solenoid and magnet spectrometer system (acceptance study $m(\pi\pi\pi) < 1.6$ GeV/c^2)," No. 43-II (October 1970).
   d. "Solenoid reconstruction errors due to axial B field," No. 43-III (November 1970).
   e. "Algorithm for track searching in solenoid spark chambers," No. 43-IV (November 1970).
   f. "P_T, P_L, and $m(\pi\pi\pi) > 2$ GeV/c kinematics for real data and Monte Carlo data," No. 43-V (November 1970).
   g. "Solenoid high mass acceptance for $\pi p \rightarrow \pi\pi\pi p$," No. 43-VI (December 1970).
   h. "B_z, B_r inside the solenoid, box approximation vs exact calculation" with C. Stoner, No. 43-VII (December 1970).
   i. "Acceptance vs magnet aperture," No. 48 (July 1970).

3. J. Ballam, A. D. Brody, G. B. Chadwick, Z.G.T. Guiragossian, W. B. Johnson, R. R. Larsen, D.W.G.S. Leith and K. Moriyasu, Report Nos. SLAC-PUB-475, -627, and -900, Stanford Linear Accelerator Center, Stanford University, Stanford, California.
4. See for example, D. B. Smith, R. J. Sprafka, and J. A. Anderson, Phys. Rev. Letters 23, 1064 (1969) or L. Van Hove, Physics Reports 1, 347 (1971).
5. A Monte Carlo program originally written at Johns Hopkins University by Dan Gillespie is used. For the higher mass studies, a CERN program called GENIS is used because of its more realistic and efficient use of the P_T momentum spectrum.
6. TVGP circle fitting procedure known as "Ascoli's method" was used. It was run in a double precision mode.
7. Ge Deng, SLAC, October 1970, a new coil program COIL II. H. Brechna at SLAC proposed this first approximation of the solenoid coil configuration.